Cell Metabolism

Article

Mitochondrial metabolism regulates the immunogenic responsiveness of dendritic cells

Graphical abstract

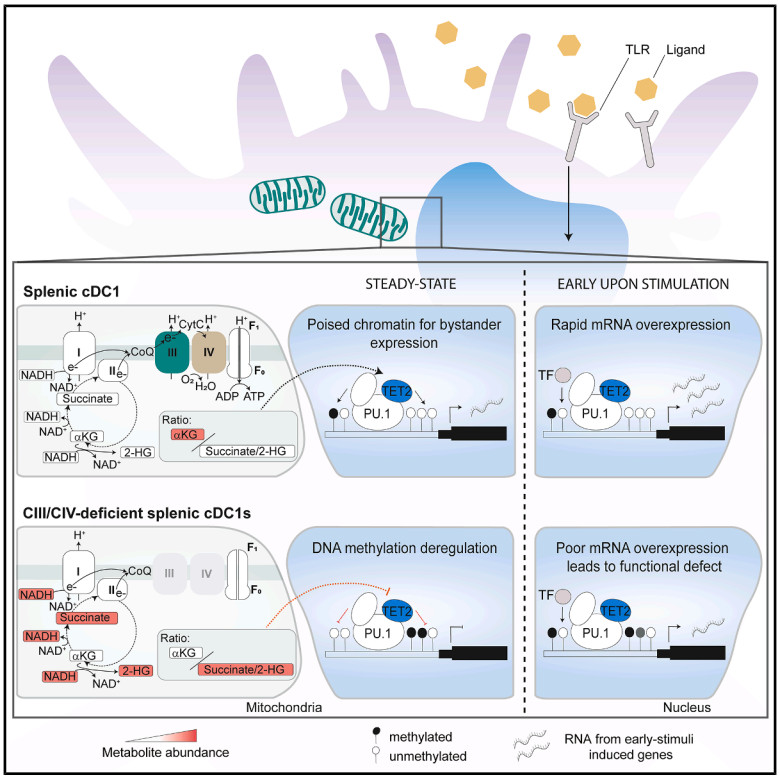

Highlights

- ETC/OXPHOS activity preferentially primes cDC1s for fast, immunogenic activation
- ETC impairment decreases cDC1 co-stimulation, migration, and T cell priming capacity
- CIII loss skews cDC1 DNA methylation and lowers expression of immunogenic genes
- Metabolite balance, not ATP, poises cDC1 epigenome for rapid stimulus response

Authors

Ignacio Heras-Murillo, Diego Mañanes, Josep Calafell-Segura, ..., Esteban Ballestar, Stefanie K. Wculek, David Sancho

Correspondence

stefanie.wculek@irbbarcelona.org (S.K.W.),
dsancho@cnic.es (D.S.)

In brief

How metabolism shapes dendritic cell (DC) immunogenicity is debated—while glycolysis activates, OXPHOS implies tolerance. Heras-Murillo et al. find that ETC electron flow primes cDC1s via redox/metabolite balance and PU.1/AP-1-tuned DNA methylation; complex III loss blunts activation and T cell priming, rescued by alternative oxidase and phenocopied by TET2 deficiency.

Heras-Murillo et al., 2026, Cell Metabolism *38*, 1097–1112
June 2, 2026
https://doi.org/10.1016/j.cmet.2026.03.012

CellPress

Cell Metabolism

CellPress
OPEN ACCESS

Article

Mitochondrial metabolism regulates the immunogenic responsiveness of dendritic cells

Ignacio Heras-Murillo,[1] Diego Mañanes,[1,2] Josep Calafell-Segura,[3] Adrián Belinchón García,[1] Clara Borràs-Eroles,[4] Pablo Munné,[1,2] Annalaura Mastrangelo,[1] Sarai Martínez-Cano,[1,5] Pablo Hernansanz-Agustín,[1,6] María A. Zuriaga,[1] José J. Fuster,[1,7] Marten Szibor,[8,9] Ignacio Melero,[10,11,16] José Antonio Enríquez,[1,12] Navdeep S. Chandel,[13,14] Esteban Ballestar,[3,15] Stefanie K. Wculek,[1,4,17,*] and David Sancho[1,17,18,*]

[1]Centro Nacional de Investigaciones Cardiovasculares Carlos III (CNIC), Madrid, Spain
[2]Universidad Autónoma de Madrid, Escuela de Doctorado, Madrid, Spain
[3]Epigenetics and Immune Disease Group, Josep Carreras Leukaemia Research Institute (IJC), 08916 Barcelona, Spain
[4]Institute for Research in Biomedicine (IRB Barcelona), The Barcelona Institute of Science and Technology (BIST), Barcelona, Spain
[5]Inmunotek S.L., Alcalá de Henares, Spain
[6]Centro de Neurociencias Cajal (CNC), Alcalá de Henares, Spain
[7]CIBER en Enfermedades Cardiovasculares (CIBER-CV), Madrid, Spain
[8]Faculty of Medicine and Health Technology, Tampere University, Tampere, Finland
[9]Department of Cardiothoracic Surgery, Center for Sepsis Control and Care (CSCC), Jena University Hospital, Jena, Germany
[10]Program of Immunology and Immunotherapy, CIMA Universidad de Navarra, Pamplona, Spain
[11]Nuffield Department of Medicine, University of Oxford, Oxford, UK
[12]Centro de Investigaciones Biomédicas en Red en Fragilidad y Envejecimiento Saludable (CIBERFES), Madrid, Spain
[13]Department of Medicine, Northwestern University Feinberg School of Medicine, Chicago, IL, USA
[14]Chan Zuckerberg Biohub, Chicago, IL 60642, USA
[15]Epigenetics in Inflammatory and Metabolic Diseases Laboratory, Health Science Center (HSC), East China Normal University (ECNU), Shanghai 200241, China
[16]Navarra Institute for Health Research (IDISNA), CIBERONC, Pamplona, Spain
[17]Senior author
[18]Lead contact
*Correspondence: stefanie.wculek@irbbarcelona.org (S.K.W.), dsancho@cnic.es (D.S.)
https://doi.org/10.1016/j.cmet.2026.03.012

SUMMARY

Activation of conventional dendritic cells (cDCs) favors increased glycolysis-driven lactic fermentation, while oxidative phosphorylation (OXPHOS) links to tolerance. Here, selective targeting of the mitochondrial electron transport chain (ETC) in cDCs uncovers a critical role for OXPHOS in regulating their immunogenicity. Disruption of ETC complex III dampens adjuvant-triggered primary human and mouse cDC1 activation and their capability to prime T cells for anti-cancer immunity, while it has a milder effect on cDC2s. Mechanistically, complex III impairment in cDC1s leads to a dysregulated redox and metabolite balance, altering DNA methylation of PU.1 and activator-protein-1 (AP-1) binding regions. These epigenetic changes hinder the rapid induction of immediate-early stimulus-induced genes in cDC1s upon stimulation. The reduced immunogenic responsiveness of ETC-impaired cDC1s can be rescued by ectopic expression of alternative oxidase and phenocopied by *Tet2* deficiency. Our findings reveal that electron flow through the ETC maintains a poised activation state in cDC1s, essential for effective anti-tumor immunity.

INTRODUCTION

Dendritic cells (DCs) orchestrate the crosstalk between innate and adaptive immunity. Conventional DCs (cDCs) are ontogenically subdivided into type 1 (cDC1s) and type 2 (cDC2s) and excel at antigen presentation and naive T cell priming upon immunogenic stimulation. DC activation is triggered by pathogen recognition receptor (PRR) signaling and involves their rapid responses to elevate co-stimulatory molecule expression and cytokine secretion and migrate to T cell zones. cDC1s are particularly potent in stimulating $CD8^+$ T cell and $CD4^+$ T helper type 1 (Th1) cell responses and hence vital for protection against viral infection and cancer.[1,2]

Cellular metabolism has emerged as an essential factor controlling DC development and function, and it is therefore a potential therapeutic target.[3–5] Glycolysis-derived pyruvate can be fermented to lactate or oxidized to CO_2 in the mitochondrial tricarboxylic acid (TCA) cycle. Glycolysis/lactic fermentation occur in the cytosol, while the mitochondrial electron transport chain (ETC), which consists of four complexes (CI–CIV), generates the driving force for oxidative phosphorylation (OXPHOS) to produce ATP at complex V (CV).[6] Lactic

fermentation re-oxidizes NADH that was generated during glycolysis in the cytoplasm to allow the glycolytic flux, while the mitochondrial ETC re-oxidizes NADH that was generated by the TCA cycle to maintain the TCA cycle flux. In that way, glycolysis-driven fermentation and oxidation-linked respiration are the main energy-generating pathways of eukaryotic cells. Steady-state cDC1s from mouse spleen are bioenergetically more active than cDC2s, with comparatively higher rates of glycolysis, mitochondrial respiration, and dependency on OXPHOS-derived ATP.[7–10] A transversal feature across DC models in mouse and humans is the persistent increase in glycolytic flux linked to lactic fermentation upon immunogenic stimulation, which is required for DC effector functions.[11–14] Decreases in hypoxia-inducible factor 1-alpha (HIF1α)-driven glycolysis in DCs at later stages are associated with their decreased migration[15] but elevated T cell activation capacity.[16]

In contrast, OXPHOS metabolism is largely associated with immunosuppressive features of DCs. Tolerogenic human monocyte-derived DCs (moDCs) rely on a fatty acid oxidation (FAO)-driven OXPHOS metabolism for their immunosuppressive phenotype.[3,10,17,18] In the steady state, mitochondrial ETC dysfunction upon aging and inhibition of the ETC correlates with decreased phagocytic activity of splenic mouse cDC subsets.[19] Mouse DC-like cells, differentiated in culture with granulocyte-macrophage colony-stimulating factor (GM-CSF) (GMDCs), increase their mitochondrial respiration shortly after immunogenic stimulation, but at longer time points, OXPHOS is blocked by a nitric oxide (NO)-dependent mechanism.[11,20] Notably, cDC1s and cDC2s lack the expression of the NO-producing enzyme iNOS upon activation.[20] Despite the distinct functional specialization of naturally occurring cDC1 and cDC2 subsets,[1,2] their respective dependency on mitochondrial metabolism, its relevance for their immunogenic functions, and the mechanistic underpinnings are poorly explored.

Here, we demonstrate that cDC1s require intact OXPHOS to accelerate their responses upon immunogenic activation. Disruption of the ETC, either through genetic deletion or pharmacological inhibition of a component of CIII, impairs the response of both human and mouse cDCs to PRR stimulation, with graded effects across cDC subsets. Specifically, CIII-impaired cDC1s show reduced upregulation of co-stimulatory molecules, impaired migration, and diminished T cell priming and anti-cancer capacity upon activation, due to delayed induction of immediate-early stimulus-induced genes. In contrast, cDC2s are less affected by CIII dysfunction. Mechanistically, cDC1s rely on a running ETC not primarily for ATP production but to maintain redox (NAD^+/NADH ratio) and metabolite balance. This metabolic state maintains a poised epigenetic DNA methylation state of PU.1- and activator-protein-1 (AP-1)-controlled genes in cDC1s, which enables rapid transcriptional responses upon immunogenic activation.

RESULTS

Immunogenic activation induces differential remodeling of mitochondrial respiration in cDC1s compared with cDC2s

First, we evaluated parameters of mitochondrial OXPHOS in cDC1s vs. cDC2s in the steady state and after PRR stimulation. Consistent with previous findings,[7] OXPHOS-related gene expression was significantly elevated in splenic cDC1s vs. cDC2s[21] (Figure S1A), and cDC1s from Flt3L-differentiated DC cultures (FLDCs) displayed an increased mitochondrial membrane potential (MMP), compared with cDC2s, at baseline (Figure S1B). Next, we purified cDC1s and cDC2s from FLDCs and treated them for 1, 4, or 20 h with the PRR agonists CpG-ODN1826 (for Toll-like receptor 9 [TLR9], expressed by both cDC subsets), poly(I:C) (PIC) (for TLR3, mainly expressed by cDC1s), and R848 (for TLR7/8, mainly expressed by cDC2s).[1,2] In line with previous reports,[11,22] activation led to a sustained increase of the extracellular acidification rate (ECAR) (Figures S1C–S1F). Notably, stimulation of cDC1s caused a persistent increase of their basal and maximal respiratory rate (BRR and MRR, indicators of ETC activity), while the ECAR/oxygen consumption rate (OCR) ratio remained unchanged at early time points and decreased at longer time points, suggesting that cDC1s do not switch to lactic fermentation after stimulation. Oxygen consumption by cDC2s did not show this increase upon longer stimulation (Figures 1A and S1C–S1F). The MMP of mouse splenic cDC1s was also elevated 20 h after *in vivo* stimulation with PIC (Figure S1G).

These results show the differential mitochondrial respiration of cDC subtypes upon TLR triggering with persistently enhanced mitochondrial activity uniquely in cDC1s, contrary to observations with GMDCs[20] and total splenic $CD11c^+$ DCs.[22]

ETC impairment hampers splenic cDC1 functions upon activation, including their capacity to stimulate anti-cancer immunity

Next, we aimed to determine the relevance of an active ETC for the main activities of cDC subsets after immunogenic stimulation *in vivo*. CIII controls the redox state of coenzyme Q as the first essential complex to accept electrons that entered the ETC and is, therefore, key to OXPHOS.[23] Thus, we sought to impair CIII as a means to interrogate the role of the ETC in cDCs. For that, we crossed *Itgax*^{Cre}[24] with *Uqcrq*$^{f/f}$[23] (*Itgax*Δ*Uqcrq*) mice to delete the subunit VII from ubiquinol-cytochrome *c* reductase CIII (*Uqcrq* gene, QPC protein) in CD11c-expressing cells (Figure 1B). *Uqcrq* mRNA was effectively depleted in splenic cDC1s as well as cDC2s (Figure 1C). In line, CIII dimers and supercomplexes and mitochondrial respiration (BRR and MRR) were significantly impaired, although not totally blocked, in total splenic $CD11c^+$ cDCs from *Itgax*Δ*Uqcrq* compared with *Uqcrq*$^{f/f}$ mice (Figures 1D, 1E, S1H, and S1I). The increased ECAR/OCR indicates enhanced lactic fermentation in *Uqcrq*-deficient cDCs (Figure S1I). These changes occurred without alteration in mitochondrial DNA content (Figure S1J). *Uqcrq* deletion in CD11c-expressing cells did not impact spleen cellularity or the numbers of resident cDC1s and cDC2s in the spleen and inguinal lymph nodes (LNs) (Figures S1K–S1M), which makes *Uqcrq*$^{f/f}$ and *Itgax*Δ*Uqcrq* mice an optimal model to study the impact of partial impairment of mitochondrial respiration on cDC functions.

First, the capacity of unstimulated or stimulated splenic *Uqcrq*$^{f/f}$ and *Itgax*Δ*Uqcrq* cDC1s and cDC2s to take up fluorescent dextramers (endocytosis) or irradiated dead CFSE-labeled cancer cells (phagocytosis) was largely intact (Figures S2A–S2D). Second, we assessed the expression of chemokine receptors, major histocompatibility complex

CellPress
OPEN ACCESS

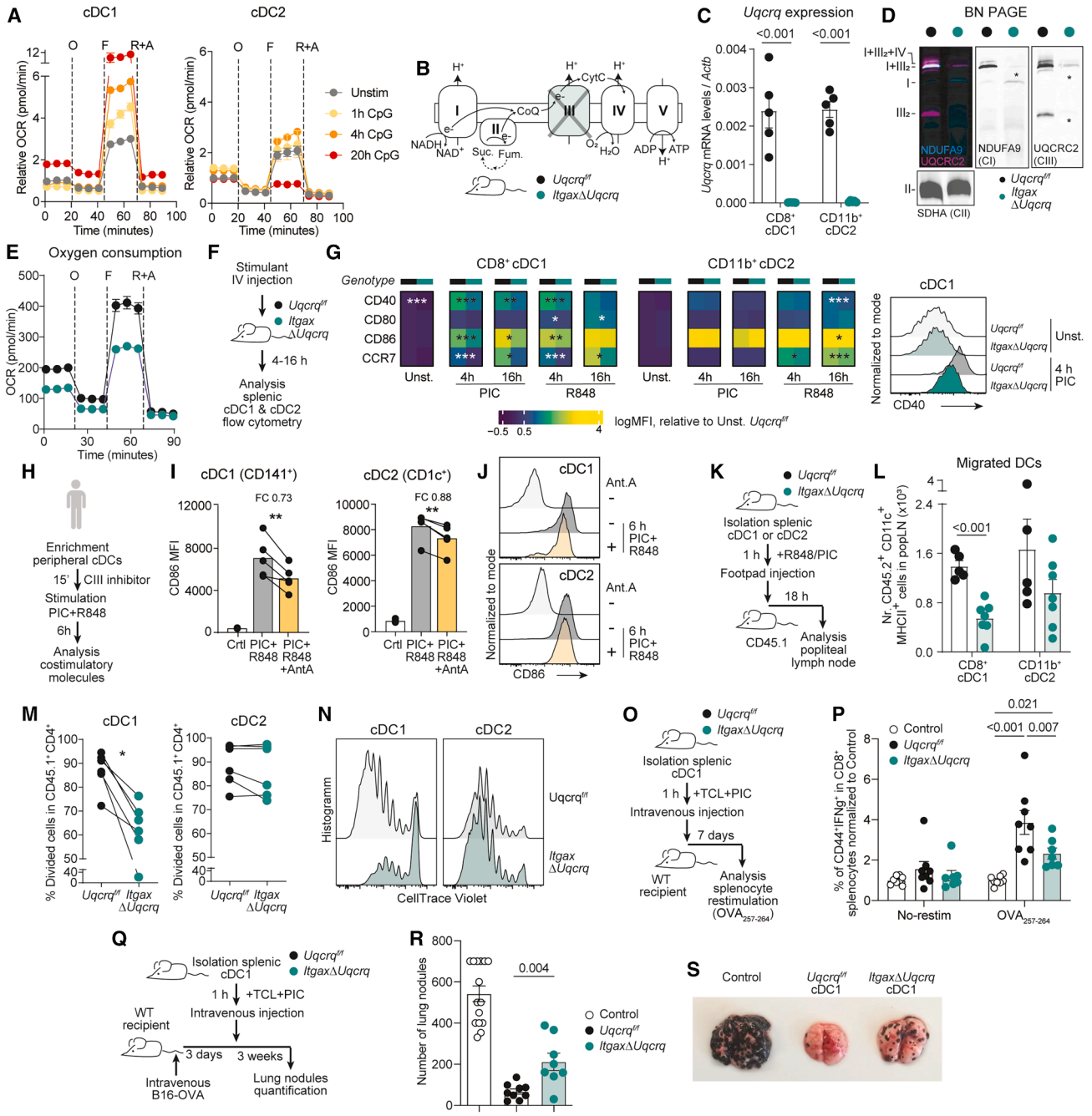

Figure 1. CIII impairment selectively dampens the responsiveness of primary cDC1s to immunogenic activation and impairs their capacity to prime cancer-controlling T cell responses

(A) Representative OCR of XCR1$^+$ cDC1s (left) or SIRPα$^+$ cDC2s (right) purified from FLDC cultures (cDCs differentiated from bone marrow by treatment with Flt3L) and stimulated or not with CpG-ODN for 1, 4, or 20 h (n = 3–5). O, oligomycin; F, FCCP; R+A, rotenone and antimycin A (Ant.A).

(B) Schematic representation of the ETC. ETC CIII, impaired in cDCs of *Itgax*Δ*Uqcrq* mice, is highlighted.

(C) *Uqcrq* expression in splenic *Uqcrq*$^{f/f}$ and *Itgax*Δ*Uqcrq* CD11c$^+$ MHCII$^+$ CD8a$^+$ cDC1s and CD11b$^+$ cDC2s ($n \geq 3$).

(D and E) Splenic CD11c$^+$ cells were purified from B16-Flt3L tumor-bearing *Uqcrq*$^{f/f}$ and *Itgax*Δ*Uqcrq* mice, and the following analyses were performed: (D) mitoplast blue native gel electrophoresis (BNGE) followed by immunodetection of NDUFA9 and UQCRC2 is shown as representative from three biological replicates. SDHA was used as loading control. (E) Mito stress test. Representative OCR is shown.

(F) Experimental overview: *Uqcrq*$^{f/f}$ and *Itgax*Δ*Uqcrq* mice were intravenously injected with R848 or PIC or control PBS, and the median fluorescence intensity (MFI) of indicated activation-associated surface molecules on splenic CD8a$^+$ cDC1s and CD11b$^+$ cDC2s was measured by flow cytometry after 4 or 16 h.

(G) Heatmap showing the average MFIs relative to cDC1s or cDC2s from PBS-treated *Uqcrq*$^{f/f}$ mice and representative histogram (gated on CD11c$^+$ MHCII$^+$ and CD8a$^+$ or CD11b$^+$ cells) of CD40 expression by cDCs after stimulating mice with PIC (cDC1) or R848 (cDC2) ($n \geq 3$) for 4 h.

(legend continued on next page)

(MHC), and co-stimulatory or co-inhibitory molecules on splenic cDC1s and cDC2s from *Uqcrq*$^{f/f}$ and *Itgax*Δ*Uqcrq* mice in steady state or upon stimulation *ex vivo* with PIC, R848, or CpG. *Itgax*Δ*Uqcrq* cDC1s displayed a strongly impaired upregulation of almost all examined DC activation-associated surface molecules upon stimulation with every TLR agonist, compared with controls. Notably, the expression of activation markers by activated *Uqcrq*-deficient cDC2s was less affected (Figures S3A–S3C). To confirm that ETC/OXPHOS disruption hinders the immunogenic activation of cDCs, we generated mice with a deletion of *Cox10* that encodes a core component of CIV[25] in cDCs (*Itgax*Δ*Cox10*) (Figure S3D). CD11c$^+$ spleen cells from *Itgax*Δ*Cox10* mice displayed decreased *Cox10* mRNA levels, CIV protein abundance, and MRR (Figures S3E–S3G), while the number of splenic cDC1s and cDC2s remained unaltered when compared with *Cox10*$^{f/f}$ controls (Figure S3H). Notably, *ex vivo* stimulation with TLR ligands also impaired the activation of splenic *Cox10*-deficient cDC1s and cDC2s, with a more profound effect in cDC1s (Figures S3I and S3J).

As *Uqcrq* depletion had a stronger effect on blocking the ETC/OXPHOS and subsequently cDC activation than *Cox10* loss, we next interrogated the functionality of CIII-impaired cDCs *in vivo*. Stimulation of *Uqcrq*$^{f/f}$ and *Itgax*Δ*Uqcrq* mice intravenously with R848, PIC, or PBS control for 4 or 16 h showed that splenic *Uqcrq*-deficient cDC1s were also unable to upregulate co-stimulatory molecule expression, compared with control littermates, while cDC2s displayed a buffered response (Figures 1F, 1G, and S3K). In line, inguinal LN (iLN)-resident *Itgax*Δ*Uqcrq* cDC1s, but to a lesser degree cDC2s, also expressed lower levels of activation markers after 4-h *in vivo* stimulation than *Uqcrq*$^{f/f}$ cDCs (Figures S3L and S3M). Treatment of wild-type splenic cDC1s and cDC2s *ex vivo* with the CIII inhibitors antimycin A or myxothiazol notably prevented the induction of activation markers upon stimulation with PIC + R848 (Figures S3N and S3O). This effect in both cDC subsets is likely due to a stronger CIII blockade by pharmacological compounds than the relatively milder effect in respiration by genetic *Uqcrq* deletion (Figure 1E), which results in a more dominant effect in cDC1s. Consistently, we confirmed the impeding effect of CIII dysfunction on the upregulation of co-stimulatory molecules upon immunogenic activation in human cDC1s and cDC2s by treating peripheral DCs from healthy human donors with CIII inhibitors before stimulation and analysis after 6-h culture (Figures 1H–1J and S3P). Finally, we investigated the intrinsic migratory potential of activated splenic cDCs from *Uqcrq*$^{f/f}$ and *Itgax*Δ*Uqcrq* mice. Significantly lower numbers *Uqcrq*-deficient cDC1s migrated to the draining LNs after adoptive transfer into the footpad, compared with their *Uqcrq*$^{f/f}$ counterparts, while cDC2s appeared largely unaffected (Figures 1K and 1L). This is in line with the impaired upregulation of CCR7 mainly on stimulated cDC1s (Figure 1F), which directs cDC migration to LNs.[26]

Next, we evaluated whether the limited immunogenic responsiveness of OXPHOS-impaired cDC1s affected their capacity to initiate T cell responses. First, we analyzed the presence of T and B lymphocytes in *Uqcrq*$^{f/f}$ and *Itgax*Δ*Uqcrq* mice. We observed unaltered numbers of B cells and total splenic CD4$^+$ T cells, while the abundance of regulatory CD4$^+$ FOXP3$^+$ T cells was decreased in the spleen, but not iLNs, of *Itgax*Δ*Uqcrq* mice (Figures S4A–S4C). Notably, the numbers of activated CD44$^+$ CD8$^+$ T cells were consistently decreased in the spleen and iLN of *Itgax*Δ*Uqcrq* mice (Figure S4A), indicating that CIII impairment in cDCs may impact their capacity to activate T cells. To specifically evaluate this, splenic *Uqcrq*$^{f/f}$ and *Itgax*Δ*Uqcrq* cDC1s and cDC2s were *ex vivo* loaded with OVA protein, stimulated, and co-cultured with naive CD4$^+$ T cells expressing an $OVA_{323–339}$ peptide-specific TCR (OT-II cells). While *Uqcrq*-deficient cDC2s were not affected, *Uqcrq*-deficient cDC1s showed a significant decrease in induction of OT-II proliferation, compared with control cDC1s, a process that is dependent on co-stimulation by antigen-presenting cells[27] (Figures 1M and 1N). Of note, the concentrations of the anti-inflammatory cytokine interleukin (IL)-10 in those cDC-OT-II co-cultures remained

(H) Experimental overview: CD141$^+$ cDC1s and CD1c$^+$ cDC2s were enriched from peripheral blood of healthy human volunteers and treated or not with Ant.A for 15 min. Then, cDCs were cultured with or without PIC and R848 for 6 h and analyzed by flow cytometry.
(I and J) MFI (I) of surface CD86 expression on CD141$^+$ cDC1s and CD1c$^+$ cDC2s and representative histogram (J) are shown (gated on HLADR$^+$ CD141$^+$ for cDC1 and HLADR$^+$CD1c$^+$ for cDC2) (n = 5).
(K) Experimental overview: splenic CD8a$^+$ cDC1s and CD11b$^+$ cDC2s were purified from B16-Flt3L tumor-bearing *Uqcrq*$^{f/f}$ and *Itgax*Δ*Uqcrq* mice (CD45.2-expressing), cultured with PIC and R848 for 1 h and injected into the footpad of CD45.1-expressing mice. After 18 h, the popliteal LN of recipient mice was analyzed by flow cytometry.
(L) Number of CD45.2$^+$ cDC1s or cDC2s ($n \geq 5$).
(M and N) OVA protein-loaded and PIC+R848-treated splenic CD11c$^+$ MHCII$^+$ CD8a$^+$ cDC1s or CD11b$^+$ cDC2s from *Uqcrq*$^{f/f}$ and *Itgax*Δ*Uqcrq* mice were co-cultured with cell trace violet (CTV)-labeled naive OVA-specific CD62L$^+$ CD44$^-$ CD4$^+$ T cells (OT-II), and T cell proliferation was assessed 5 days later by flow cytometry. (M) Frequency of CTV-diluted (proliferated) OT-II cells (n = 6) and (N) representative histogram (gated on CD45.1$^+$ CD4$^+$ cells).
(O) Experimental overview: splenic cDC1s were purified from B16-Flt3L tumor-bearing *Uqcrq*$^{f/f}$ and *Itgax*Δ*Uqcrq* mice, cultured for 1 h with PIC and B16-OVA tumor cell lysate (TCL) and injected intravenously into wild-type recipient mice. Control mice were injected with PBS. The resulting effector CD8$^+$ T cell response was assessed 7 days later by splenocyte restimulation with $OVA_{257–264}$ peptide.
(P) Frequency of endogenous CD44$^+$ IFN-γ$^+$ in total CD8$^+$ T cells in the spleen upon restimulation (n = 8).
(Q) Experimental overview: PIC and B16-OVA TCL-treated splenic cDC1s from *Uqcrq*$^{f/f}$ and *Itgax*Δ*Uqcrq* mice were generated as in (O) and injected intravenously into wild-type recipients that had received an intravenous injection of B16-OVA 3 days before. Control mice were injected with PBS.
(R and S) Quantification of melanoma nodules in the lung (n = 8) (R) and representative lung images (S) 21 days after tumor inoculation.
Data are presented as mean in heatmaps or mean ± SEM (dots represent individual data points) and pooled from at least two independent experiments (A–G and K–S), or data represent different human donors (H–J). Statistical analysis by two-way unpaired Student's t test (C), two-way ANOVA with Sidak post hoc testing between cDCs from *Uqcrq*$^{f/f}$ and *Itgax*Δ*Uqcrq* mice (G) or groups (P), paired Student's t test (I and M), multiple unpaired Student's t test (L), and one-way ANOVA (R). $^*p \leq 0.05$, $^{**}p \leq 0.01$, $^{***}p \leq 0.001$.
See also Figures S1–S4.

CellPress
OPEN ACCESS

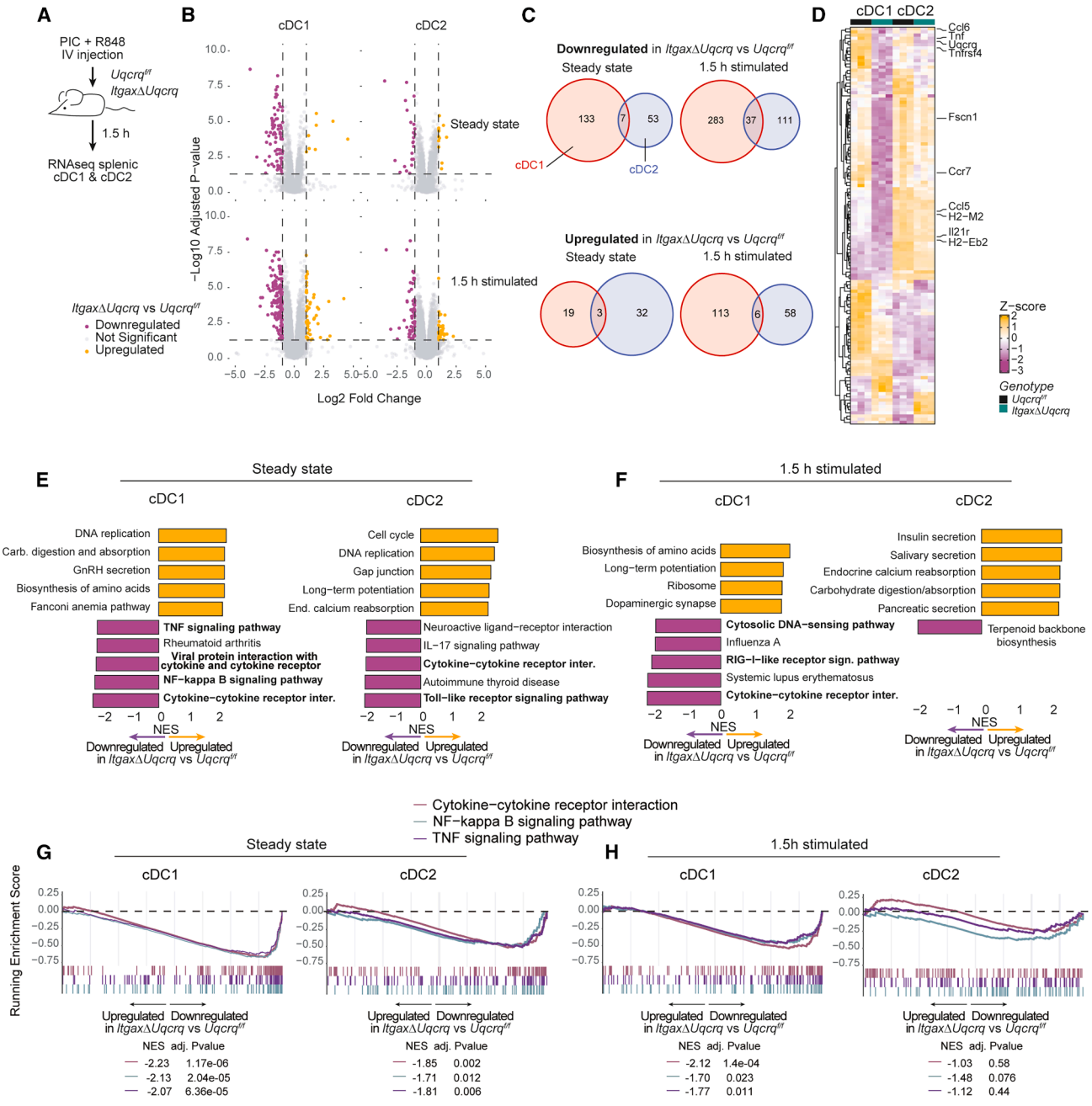

Figure 2. CIII dysfunction globally downregulates the expression of immune function-related genes in cDC1s

(A) Experimental overview of (B)–(H): *Uqcrq*$^{f/f}$ and *ItgaxΔUqcrq* mice were intravenously injected with PIC + R848 (1.5 h stimulated) or PBS as control (steady state), and after 1.5 h, splenic CD11c^{+} MHCII^{+} CD8a^{+} cDC1s or CD11b^{+} cDC2s were subjected to RNA-seq (n = 3 from 3 independent experiments).

(B) Volcano plot of genes expressed by *ItgaxΔUqcrq* vs. *Uqcrq*$^{f/f}$ cDC1s (left) or cDC2s (right), unstimulated (top) or after 1.5 h stimulation (bottom). Differentially expressed genes (DEGs) (abs(logFC > 1) and adjusted $p \leq 0.05$) are highlighted.

(C) Venn diagram depicting the number of downregulated or upregulated DEGs (top and bottom, respectively) comparing *Uqcrq*-deficient with control cDC1s (red) or cDC2s (blue) in the steady state or upon stimulation with their overlap.

(D) Heatmap of relative expression of DEGs between *ItgaxΔUqcrq* vs. *Uqcrq*$^{f/f}$ unstimulated cDC1s and cDC2s. Key DC activation-associated genes are highlighted.

(E and F) Pre-ranked GSEA. Significantly (adjusted $p \leq 0.02$) downregulated (purple) or upregulated (orange) pathways (Kyoto Encyclopedia of Genes and Genomes [KEGG] database) including normalized enrichment score (NES) in splenic cDC1s or cDC2s from steady-state (E) or stimulated *ItgaxΔUqcrq* vs. *Uqcrq*$^{f/f}$ mice (F). Bold pathways are related to immunogenic activation or function of DCs. All or the five most significantly dysregulated pathways are shown.

(G and H) Barcode plots ranking the expression of genes by logFC from high (left) to low (right) in *ItgaxΔUqcrq* compared with *Uqcrq*$^{f/f}$ cDC1s or cDC2s. Running enrichment scores of genes included in the "cytokine-cytokine receptor interaction" (magenta), "nuclear factor κB (NF-κB) signaling pathway" (teal), and "tumor

(legend continued on next page)

unaffected by *Uqcrq*-deficiency of cDCs (Figure S4D), suggesting that, foremost, the immunogenic $CD4^+$ T cell activation by CIII-impaired cDC1s is compromised. cDC1s excel at cross presentation of exogenous antigens on MHC-I molecules to prime $CD8^+$ T cells.[1] To address this capacity of cDC1s with a dysfunctional CIII *in vivo*, we performed adoptive transfer experiments of *ex vivo* B16-OVA tumor antigen-loaded and stimulated cDC1s from $Uqcrq^{f/f}$ and *Itgax*Δ*Uqcrq* mice into wild-type recipient mice (anti-cancer vaccines).[28] Then, 7 days thereafter, we analyzed the OVA-specific T cell response upon restimulation and found that mice vaccinated with *Uqcrq*-deficient cDC1s harbored a significantly decreased frequency of endogenous activated $CD44^+$ interferon (IFN)-γ^+ $CD8^+$ T cells, compared with controls (Figures 1O and 1P). Those results highlight a decreased intrinsic capacity of cDC1s with an impaired ETC to prime effector T cell responses, which may impact the therapeutic efficacy of cDC1-based anti-cancer vaccines. To address this, we transferred B16-OVA tumor antigen-loaded and stimulated cDC1s from $Uqcrq^{f/f}$ and *Itgax*Δ*Uqcrq* mice into recipients that were previously injected intravenously with B16-OVA melanoma cells. $Uqcrq^{f/f}$ cDC1s effectively decreased the growth of experimental metastases in the lung, compared with control mice; however, CIII-impaired cDC1s were significantly less potent to do so (Figures 1Q–1S).

Overall, these results indicate that cDC1s are highly dependent on an intact ETC for effective activation, upregulation of co-stimulatory molecules, migration and optimal T cell priming, and anti-cancer immunity. cDC2s exhibit a milder phenotype and appear to rely less on mitochondrial respiration than cDC1s for their immunogenic responsiveness.

Expression of immunogenic function-related genes by activated cDC1s requires an intact mitochondrial respiration

To investigate how ETC impairment affects cDC activation, we performed transcriptional profiling of splenic cDC1s or cDC2s from $Uqcrq^{f/f}$ and *Itgax*Δ*Uqcrq* mice by RNA sequencing (RNA-seq), both at steady state and upon *in vivo* stimulation with PIC and R848 (Figure 2A). Only a small proportion of dysregulated genes was shared between *Uqcrq*-deficient cDC1s and cDC2s; and cDC1s were generally more strongly affected. In particular, a high number of genes were significantly downregulated in *Itgax*Δ*Uqcrq* vs. $Uqcrq^{f/f}$ cDC1s in steady state, and the difference was even more profound after immunogenic activation (Figures 2B–2D). Pre-ranked gene set enrichment analysis (GSEA) revealed that most of the downregulated genes in *Uqcrq*-deficient cDC1s corresponded to pathways associated with immunogenic activation of DCs, such as "cytokine-cytokine receptor interaction" (Figures 2E and 2F). Notably, while some activation-related pathways were significantly reduced in *Uqcrq*-deficient cDC2s under steady-state conditions, these differences were no longer evident following stimulation. This is especially highlighted by the more consistent downregulation of genes pertaining to selected immune function-related pathways in CIII-impaired cDC1s than in cDC2s at baseline, which is only maintained significantly downregulated in *Uqcrq*-deficient cDC1s upon stimulation (Figures 2G and 2H). To further confirm these findings, we performed pathway over-representation analysis of significantly dysregulated genes in cDCs in the steady state using ingenuity pathway analysis (IPA). Immunogenic DC activation-related pathways were highly over-represented within downregulated genes in *Itgax*Δ*Uqcrq* vs. $Uqcrq^{f/f}$ cDC1s, but such pathways were not significantly enriched in dysregulated genes of *Uqcrq*-deficient cDC2s in this analysis (Figure S5A). Consistently, only CIII-impaired cDC1s displayed a decreased expression of genes within the DC maturation pathway (IPA database), which was largely normal in cDC2s of both genotypes (Figure S5B). Notably, the expression of genes associated with tolerogenic features of DCs[29] remained unaltered in *Uqcrq*-deficient cDC1s and cDC2s (Figure S5C), suggesting that they do not acquire a notable tolerogenic phenotype. Finally, to determine if CIII dysfunction impacts the identity of cDC1s or cDC2s, we analyzed the expression of cDC subset signature genes, as described previously in the literature.[30] The levels of hallmark genes for cDC1s and cDC2s were equal in splenic cDC subsets from $Uqcrq^{f/f}$ and *Itgax*Δ*Uqcrq* mice (Figure S5B).

In summary, our data show that impaired mitochondrial respiration does not alter the core identity of splenic cDC1s and cDC2s. However, under steady-state conditions, *Uqcrq*-deficient cDC1s exhibit a marked reduction in the expression of genes related to immune function, while cDC2s are less affected. After activation, gene expression in OXPHOS-impaired cDC2s is fully restored, whereas the downregulation of immunogenicity-associated genes in *Itgax*Δ*Uqcrq* cDC1s becomes even more pronounced. These findings suggest that a functional ETC is particularly critical for enabling the prompt immunogenic response of cDC1s to PRR triggering.

CIII interference in cDC1s results in altered DNA methylation that impairs the bystander expression and rapid upregulation of immediate-early immune stimulus-induced genes

The global dysregulation of immune function-related gene expression in OXPHOS-impaired cDC1s suggests the involvement of epigenetic control mechanisms. Hence, we profiled chromatin accessibility and DNA methylation status in splenic $Uqcrq^{f/f}$ and *Itgax*Δ*Uqcrq* cDC1s and cDC2s via the assay for transposase-accessible chromatin using sequencing (ATAC-seq)[31] and a cytosine methylation array, respectively (Figure 3A). Principal-component analysis (PCA) of differentially open chromatin regions, comparing cDC subsets of both genotypes, showed that most of the variability between samples was explained by differences between cDC1 and cDC2 subsets (Figure 3B). Only few alterations in chromatin accessibility were found between cDCs from $Uqcrq^{f/f}$ or *Itgax*Δ*Uqcrq* mice, and global histone H3 acetylation was also unchanged (Figures 3C, S5D, and S5E). Regarding DNA methylation changes, differential

necrosis factor (TNF) signaling pathway" (purple) gene sets from the KEGG database in the steady state (G) or upon stimulation (H) are depicted by curved solid lines. Vertical colored lines below depict the expression position of genes of each pathway within all detected genes. Dashed lines are for orientation only and indicate a running enrichment score of 0. At the bottom, NES and significance for each GSEA are indicated.
See also Figure S5.

CellPress
OPEN ACCESS

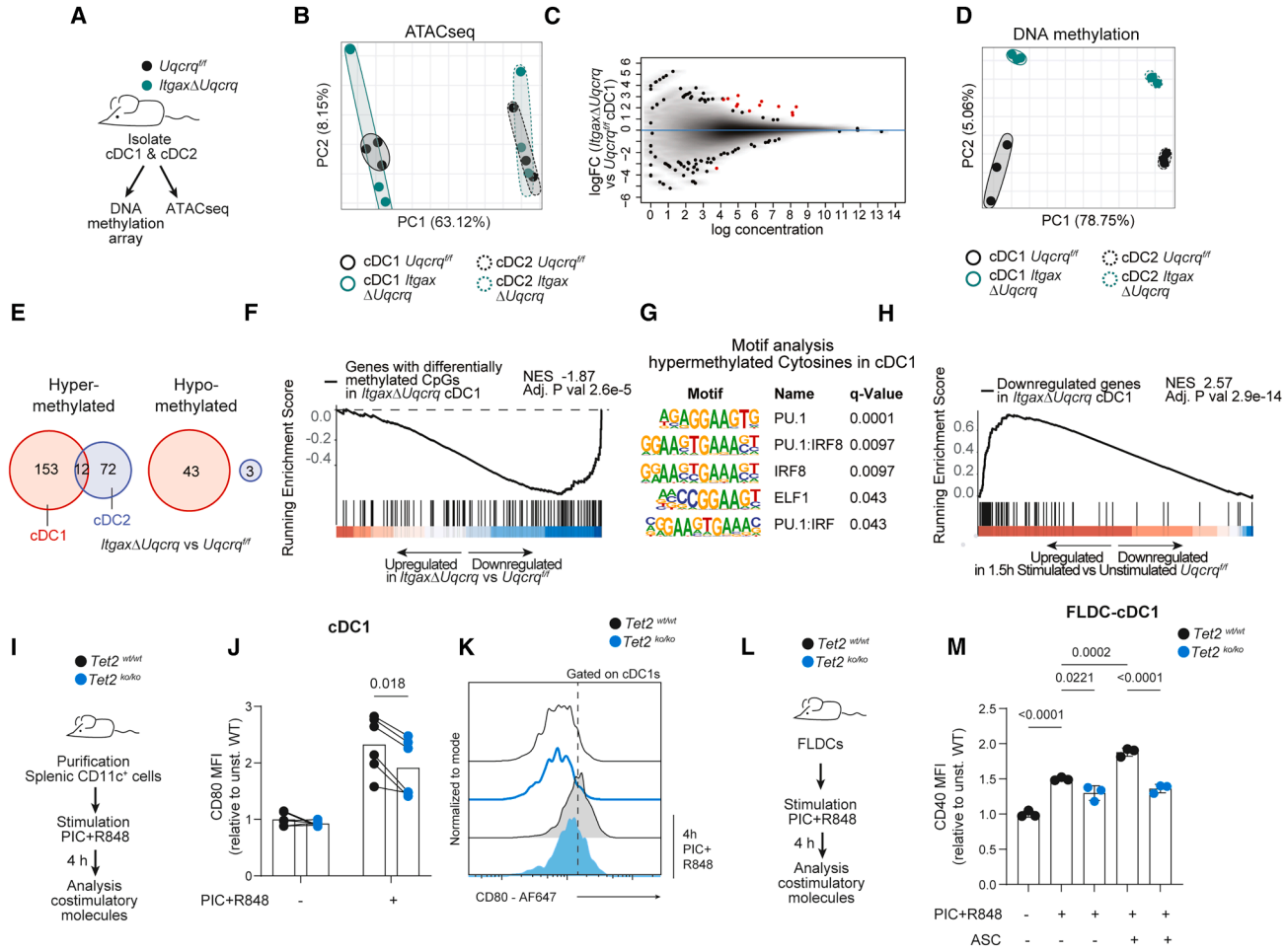

Figure 3. *Uqcrq* deficiency in cDC1s causes DNA hypermethylation at PU.1 binding sites

(A) Experimental overview of (B)–(G): splenic CD11c$^+$ MHCII$^+$ CD8a$^+$ cDC1s and CD11b$^+$ cDC2 were purified from *Uqcrq*$^{f/f}$ and *Itgax*Δ*Uqcrq* mice, and the epigenetic state of the nuclear DNA was analyzed by ATAC-seq (B and C) and DNA methylation array (D–G) (n = 3).

(B and C) PCA (B) of all differentially accessible chromatin regions (DARs, false discovery rate [FDR] $\leq$ 0.05) detected by ATAC-seq in cDC1s and cDC2s from *Itgax*Δ*Uqcrq* vs. *Uqcrq*$^{f/f}$ mice. MA plot (C) shows the differential accessibility of peaks of cDC1s from *Itgax*Δ*Uqcrq* vs. *Uqcrq*$^{f/f}$ mice.

(D and E) PCA (D) and Venn diagram (E) of all DMPs (abs(diff beta > 0.05, FDR $\leq$ 0.1)) in cDC1s and cDC2s from *Itgax*Δ*Uqcrq* compared with *Uqcrq*$^{f/f}$ mice.

(F) Barcode plot (RNA-seq data from Figure 2) ranking the expression of genes by logFC from high (left) to low (right) in steady-state *Itgax*Δ*Uqcrq* vs. *Uqcrq*$^{f/f}$ cDC1s. Running enrichment scores of genes containing DMPs are depicted by a curved solid line. Vertical black lines below depict the expression position of those within all detected genes.

(G) TF motif enrichment analysis on hypermethylated cytosines in *Uqcrq*-deficient vs. control cDC1s. Enriched known motifs, TF name(s), and enrichment significance (FDR < 0.05) are shown.

(H) Barcode plot (RNA-seq data from Figure 2) ranking the expression of genes by logFC from high (left) to low (right) in PIC + R848-stimulated vs. steady-state *Uqcrq*$^{f/f}$ cDC1s. Running enrichment scores of significantly downregulated genes (logFC < −1 and adjusted $p \leq 0.05$) in *Itgax*Δ*Uqcrq* compared with *Uqcrq*$^{f/f}$ cDC1s in the steady state are depicted by a curved solid line. Vertical black lines below depict the expression position of those within all detected genes.

(I–K) Experimental overview (I): splenic CD11c$^+$ cells from *Tet2*$^{wt/wt}$ and *Tet2*$^{ko/ko}$ mice were stimulated with PIC and R848 or control PBS, and the MFI of CD80 on splenic CD8a$^+$ cDC1s and CD11b$^+$ cDC2s was measured by flow cytometry after 4 h. Bar plot of the MFIs relative to unstimulated cDC1s from *Tet2*$^{wt/wt}$ mice (J) and representative histogram (K; gated on CD11c$^+$ MHCII$^+$CD8a$^+$CD11b$^-$) are shown (n = 6).

(L) Experimental overview: FLDCs were generated from bone marrow of *Tet2*$^{wt/wt}$ and *Tet2*$^{ko/ko}$ mice in the presence or absence of ASC. On day 9, FLDCs were stimulated with PIC and R848 or control PBS, and the MFI of CD40 was measured by flow cytometry after 4 h on XCR1$^+$ cDC1s.

(M) Bar plot of MFIs relative to unstimulated cDC1s from *Tet2*$^{wt/wt}$ mice is shown (n = 6).

Data are presented as mean ± SEM (dots represent individual data points) and pooled from at least two independent experiments. Statistical analysis by multiple paired Student's t test (J) and one-way ANOVA (M).

See also Figure S5.

features between cDC1s and cDC2s also accounted for most of the sample variability in the PCA of differentially methylated positions (DMPs) (PC1). However, PC2 distinguished samples according to genotype, showing that CIII dysfunction notably alters the DNA methylation status of cDCs, affecting *Uqcrq*-deficient cDC1s more strongly than cDC2s (Figures 3D–3G). This is consistent with the extent of downregulation of gene expression in those cDC subsets upon *Uqcrq* loss (Figure 2B). Moreover, DMPs in *Itgax*Δ*Uqcrq* cDC1s were located in genes whose expression is most downregulated in those cells compared with controls, suggesting that the dysregulation of DNA methylation is associated with the repression of gene transcription in *Uqcrq*-deficient cDC1s (Figure 3F). Notably, transcription factor (TF) motif enrichment analysis showed that hypermethylated DMPs in *Itgax*Δ*Uqcrq* cDC1s are predominantly found in the vicinity of PU.1 binding sites (Figure 3G). Conversely, no significant enrichment of TF motifs was found close to DMPs in *Uqcrq*-deficient vs. control cDC2s. PU.1 is a "pioneer" TF that binds multiple genomic regions upon differentiation of cDCs and controls the expression of immune function-related genes after cDC activation.[32–35] PU.1 is involved in stimulus-dependent induction hubs where, together with other TFs, chromatin is poised to enable a bystander gene expression and the fast transcriptional response of immediate-early stimulus-inducible genes upon DC stimulation.[36,37] Consistently, the genes that were significantly downregulated in steady-state *Itgax*Δ*Uqcrq* vs. *Uqcrq*$^{f/f}$ cDC1s (bystander expression) largely coincided with rapidly overexpressed genes in stimulated vs. unstimulated *Uqcrq*$^{f/f}$ (control) cDC1s *in vivo* (immediate-early stimulus-inducible genes) (Figure 3H).

Overall, a dysfunctional ETC causes alterations in DNA methylation in cDC1s and cDC2s, without altering chromatin accessibility. OXPHOS-impaired cDC1s are more profoundly affected than cDC2s. The altered basal methylation levels at PU.1-controlled immediate-early stimulus-inducible genes, which are related to immunogenic properties, translate into suboptimal cDC1 responsiveness to activation and their subsequent functional defects. The impact of *Uqcrq* deficiency on the epigenetic state of cDC2s is buffered, in line with the milder transcriptional and functional alterations of those cells.

PU.1 can recruit both DNA methyltransferases and methylcytosine dioxygenases, like TET2,[38,39] which mediate active DNA demethylation. We therefore used *Tet2*$^{ko/ko}$ mice to assess whether interference with DNA demethylation impacts cDC activation. We verified *Tet2* absence in CD11c^{+} cells and an unaltered frequency of cDC1s and cDC2s from the spleen of *Tet2*$^{ko/ko}$, compared with control mice (Figures S5F and S5G). Then, we assessed the activation of splenic *Tet2*-deficient cDCs upon *ex vivo* stimulation with PIC and R848 for 4 h and observed impaired upregulation of CD80 on *Tet2*$^{ko/ko}$ cDC1s and cDC2s (Figures 3I–3K and S5H). Next, we aimed to activate TET2 in cDCs by differentiating FLDCs from the bone marrow of wild type or *Tet2*$^{ko/ko}$ in the presence of L-ascorbic acid (ASC), a TET2 co-factor that can enhance its catalytic activity.[40] Again, we observed that *Tet2* deficiency impaired the upregulation of co-stimulatory molecules by cDC1s and cDC2s upon stimulation. Conversely, ASC treatment of wild-type cDC1s and cDC2s significantly increased expression of co-stimulatory molecules such as CD40, CD86, or CD80, which was largely TET2 dependent (Figures 3L, 3M, S5I, and S5J). This similar enhancement of the immunogenic responsiveness of both cDC subsets after ASC treatment suggests that the regulation of TET2 activity likely lies downstream of the graded relevance of ETC/OXPHOS metabolism between cDC1s and cDC2s.

Hence, our results suggest that *Uqcrq* deficiency in cDC1s hampers their poised DNA methylation landscape at loci close to PU.1 binding sites, likely involving TET2 activity. This epigenetic alteration leads to reduced basal gene expression and impaired induction of immediate-early stimulus-inducible genes in ETC/OXPHOS-impaired cDC1s.

Compromised metabolite and redox balances underlie the diminished activation of CIII-impaired cDC1s

Next, we mechanistically investigated how a dysfunctional CIII alters DNA methylation through analyzing the main functions of the ETC in splenic cDC1s and cDC2s from *Uqcrq*$^{f/f}$ and *Itgax*Δ*Uqcrq* mice. The ETC generates a proton gradient across the inner mitochondrial membrane that powers CV for ATP biosynthesis. CIII also contributes to reactive oxygen species (ROS) production, which may directly or indirectly affect DNA methylation deposition or removal.[41] However, ATP concentrations, the MMP, and ROS levels were comparable in *Uqcrq*$^{f/f}$ and *Itgax*Δ*Uqcrq* cDC1s and cDC2s in the steady state and after activation *in vivo* (Figures 4A–4C). This intact bioenergetics and oxidative state of *Uqcrq*-deficient cDCs are likely attributable to their remaining OXPHOS activity and compensatory mechanisms to maintain ATP production and MMP[42] (Figure 1E).

The flow of electrons through the ETC is achieved by accepting electrons (reduction), which are transferred to CIII. In their reduced form, the redox coenzyme NADH is an important cofactor for many enzymatic reactions of metabolic pathways, including the TCA cycle. Via the recycling of NADH, the ETC maintains the NAD^{+}/NADH redox balance in the cell.[43] Moreover, CII of the ETC, also known as succinate dehydrogenase, is an integral enzyme of the TCA cycle, linking ETC function to TCA cycle flow.[6] CIII dysfunction likely prevents CII activity, which additionally hampers the TCA cycle. To investigate the role of redox and metabolite balance on the dysfunction of CIII-impaired cDC1s, we partially restored the ETC in CIII-impaired cDCs, using mice constitutively expressing alternative oxidase (AOX) from *Ciona intestinalis* (*Aox*^{Rosa26} mice)[44] crossed with *Itgax*Δ*Uqcrq* mice. AOX is absent in vertebrates and can accept electrons directly from coenzyme Q to produce H_2O without pumping protons into the intermembrane space (Figure 4D). Thereby, AOX expression re-establishes the electron flux through CI and CII in CIII-impaired cells, which specifically restores redox and metabolite balance but not the generation of an MMP and ATP production.[44] Indeed, we observed an elevated oxygen consumption of splenic *Itgax*Δ*Uqcrq Aox*^{Rosa26} vs. *Itgax*Δ*Uqcrq* cDCs, which was rescued to levels of controls (Figures 4E, 4F, and S6A), indicating a re-established electron flux in CIII-impaired cDCs by AOX expression.

Having this confirmed, we next assessed the redox and TCA cycle metabolite balance in splenic cDC1s and cDC2s of *Uqcrq*$^{f/f}$, *Aox*^{Rosa26}, *Itgax*Δ*Uqcrq*, and *Itgax*Δ*Uqcrq Aox*^{Rosa26} mice (Figure 4G). Notably, while *Uqcrq*-deficient cDC2s were also mildly affected (Figure S6B), we detected a decreased NAD^{+}/NADH ratio in splenic *Itgax*Δ*Uqcrq* vs. *Uqcrq*$^{f/f}$ cDC1s,

CellPress
OPEN ACCESS

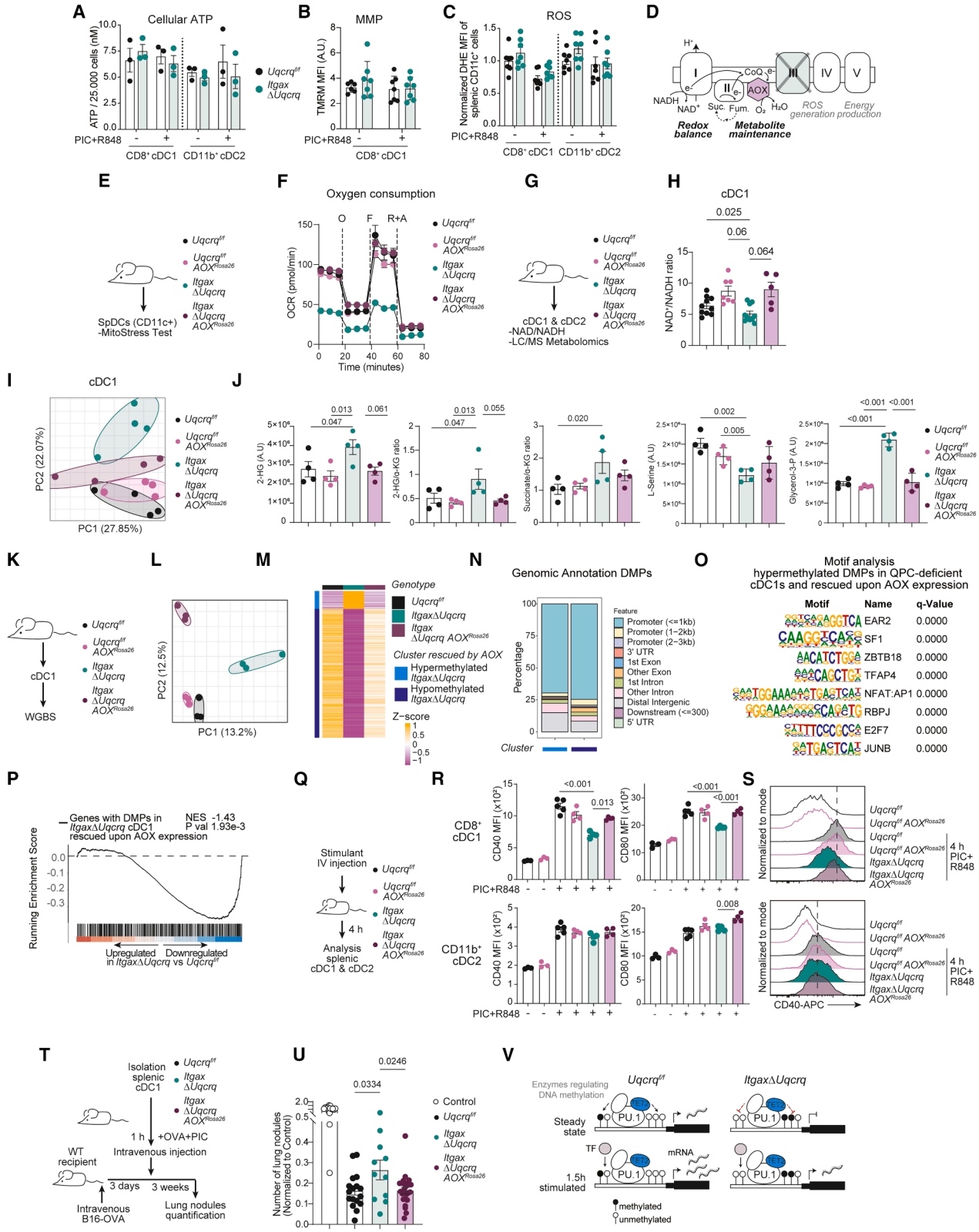

(legend on next page)

which was rescued by AOX expression (Figure 4H). We also performed targeted liquid chromatography-mass spectrometry (LC-MS) analyses to quantify more than 30 metabolites in splenic cDC1s and cDC2s (Figures 4I and S6C). The PCA of differentially abundant metabolites in cDC1s showed that *Itgax*Δ*Uqcrq* cells clustered notably distinct from *Uqcrq*$^{f/f}$ and *Aox*^{Rosa26} controls, while *Itgax*Δ*Uqcrq Aox*^{Rosa26} cDC1s had a partially rescued metabolite profile (Figures 4I, 4J, and S6D). In particular, 2-hydroxyglutarate (2-HG, a derivative of α-KG) accumulated in *Uqcrq*-deficient cDC1s and was restored to the levels of control cells upon AOX expression. In line, the 2-HG/α-KG ratio, which is critical for the activity of α-KG-dependent methylcytosine dioxygenases including TET2,[45] was elevated in *Itgax*Δ*Uqcrq* cDC1s and normalized in *Itgax*Δ*Uqcrq Aox*^{Rosa26} cDC1s. Abundance of glycerol-3-phosphate (G3P) was similarly affected in *Uqcrq*-deficient cDC1s and rescued upon AOX expression, likely due to inhibition of the G3P dehydrogenase that catalyzes the conversion of G3P to DHAP in the intermembrane space as part of the G3P shuttle for cytosolic NAD^+ recycling. Moreover, compared with *Uqcrq*$^{f/f}$ controls, *Itgax*Δ*Uqcrq* cDC1s also contained higher concentrations of succinic acid, another metabolite inhibiting α-KG-dependent TET2,[46] and lower levels of serine, an intermediate for methyl donors,[47] which were unaffected by AOX expression (Figure 4J). Notably, metabolites remained largely unaltered in cDC2s independent of their genotype (Figures S6C and S6D).

Subsequently, to analyze the effects of AOX expression on the dysregulated DNA methylation status of *Uqcrq*-deficient cDC1s, we performed whole-genome bisulfite sequencing (WGBS) of splenic cDC1s from *Uqcrq*$^{f/f}$, *Aox*^{Rosa26}, *Itgax*Δ*Uqcrq*, and *Itgax*Δ*Uqcrq Aox*^{Rosa26} mice (Figure 4K). Notably, the PCA of DMPs indicates that the altered methylation status of *Uqcrq*-deficient cDC1s is also partially rescued by AOX expression (Figure 4L). Confirming our previous results (Figure 3G), TF binding motif analysis identified enrichment of PU.1 binding sites in DMPs of *Itgax*Δ*Uqcrq* vs. *Uqcrq*$^{f/f}$ cDC1s (Figures S6E and S6F). We then interrogated the DMPs of *Uqcrq*-deficient cDC1s that were normalized by AOX expression to the state of control cDC1s and revealed hypermethylated and hypomethylated cytosines that were mostly located in the vicinity of gene promoters (Figures 4M and 4N). Notably, binding motifs of members of the AP-1 TF family (e.g., JunB and Fos) were enriched in DMPs that are hypermethylated in *Itgax*Δ*Uqcrq* cDC1s and rescued in *Itgax*Δ*Uqcrq Aox*^{Rosa26} cDC1s (Figures 4O and S6G). AP-1 members are known to be bound to immediate-early stimuli-induced genes in DCs together with PU.1 prior to stimulation[37] and are promoting immunogenic activation of DCs.[48,49] In this regard, the expression of genes containing DMPs that were rescued in *Itgax*Δ*Uqcrq Aox*^{Rosa26} cDC1s correlated with those downregulated in *Itgax*Δ*Uqcrq* cDC1s, suggesting that the AOX expression-mediated recovery of the DNA methylation landscape of cDC1s may translate into the rescue of cDC1 immunogenic function (Figure 4P).

Figure 4. CIII impairment dysregulates metabolite and redox balance in cDC1s, and re-establishment of electron flow through CI and CII rescues their immunogenic functionality

(A–C) Splenic CD11c$^+$ MHCII$^+$ CD8a$^+$ cDC1s and CD11b$^+$ cDC2s were purified from *Uqcrq*$^{f/f}$ and *Itgax*Δ*Uqcrq* mice that were intravenously treated with PIC + R848 or control PBS 4 h prior, and the following analyses were performed: quantification of intracellular ATP concentrations (A; $n = 3$), MMP by flow cytometric staining with tetramethylrhodamine methyl ester perchlorate (TMRM) (B; $n = 7$), and ROS levels by flow cytometric staining with dihydroethidium (DHE) (C; $n = 7$).

(D) Schematic representation of electron flow and the altered ETC upon CIII dysfunction and expression of ectopic AOX in transgenic AOX^{Rosa26} mice. Main functions of the ETC are indicated.

(E and F) Splenic CD11c$^+$ were purified from B16-Flt3L tumor-bearing *Uqcrq*$^{f/f}$, *Uqcrq*$^{f/f}$ *Aox*^{Rosa26}, *Itgax*Δ*Uqcrq*, and *Itgax*Δ*Uqcrq Aox*^{Rosa26} mice, and OCR was measured.

(G–J) Splenic CD11c$^+$ MHCII$^+$ CD8a$^+$ cDC1s were purified from *Uqcrq*$^{f/f}$, *Uqcrq*$^{f/f}$ *Aox*^{Rosa26}, *Itgax*Δ*Uqcrq*, and *Itgax*Δ*Uqcrq Aox*^{Rosa26} mice after hydrodynamic injection of mFLex for cDC expansion, and the following analysis was performed: calculation of NAD^+/NADH ratio after quantification of NAD^+ and NADH concentrations (H, $n = 5$–10) and quantification of 32 metabolites by LC-MS-based metabolomic profiling (I–K; $n = 4$). (I) PCA of metabolite abundance. (J) Bar plot of selected metabolites.

(K) Experimental overview: splenic CD11c$^+$ MHCII$^+$ CD8a$^+$ cDC1s were purified from *Uqcrq*$^{f/f}$, *Uqcrq*$^{f/f}$ *Aox*^{Rosa26}, *Itgax*Δ*Uqcrq*, and *Itgax*Δ*Uqcrq Aox*^{Rosa26} mice after hydrodynamic injection of mFLex for cDC expansion, and DNA methylation was analyzed by WGBS.

(L) PCA of sDMPs (abs(diff beta > 0.05, FDR $\leq$ 0.05)).

(M and N) Heatmap (M) and genomic annotation (N) of significant DMPs (abs(diff beta > 0.25, FDR $\leq$ 0.05)) in *Itgax*Δ*Uqcrq* vs. *Uqcrq*$^{f/f}$, which are significantly rescued in *Itgax*Δ*Uqcrq Aox*^{Rosa26} cDC1s. Mean β value of the three biological replicates is displayed per DMP.

(O) TF motif enrichment analysis on genomic regions containing hypermethylated DMPs in *Uqcrq*-deficient vs. control cDC1s, which are rescued in *Itgax*Δ*Uqcrq Aox*^{Rosa26}. Enriched motifs, TF name(s), and enrichment significance are shown.

(P) Barcode plot ranking the expression of genes from RNA-seq of Figure 2 by logFC from high (left) to low (right) in steady-state *Itgax*Δ*Uqcrq* vs. *Uqcrq*$^{f/f}$ cDC1s. Running enrichment scores of genes containing DMPs (abs(diff beta > 0.25, FDR $\leq$ 0.05), shown in (M), are depicted by a curved solid line. Vertical black lines below depict the expression position of those within all detected genes.

(Q) Experimental overview: *Uqcrq*$^{f/f}$, *Uqcrq*$^{f/f}$ *Aox*^{Rosa26}, *Itgax*Δ*Uqcrq*, and *Itgax*Δ*Uqcrq Aox*^{Rosa26} mice were intravenously injected with PIC + R848, and splenic CD11c$^+$ MHCII$^+$ CD8a$^+$ cDC1s and CD11b$^+$ cDC2s were analyzed 4 h later by flow cytometry.

(R and S) MFI quantification of CD40 and CD80 (R) and representative histograms (S) of CD40 are shown (gated on cDC1s [upper] or cDC2s [lower]) ($n \geq 3$).

(T) Experimental overview: PIC and OVA-treated splenic cDC1s from *Uqcrq*$^{f/f}$, *Itgax*Δ*Uqcrq*, and *Itgax*Δ*Uqcrq Aox*^{Rosa26} mice were injected intravenously into wild-type recipients that had received an intravenous injection of B16-OVA cancer cells 3 days before. Control mice were injected with PBS.

(U) Quantification of melanoma nodules in the lung normalized to untreated control 3 weeks thereafter ($n = 11$–24).

(V) Schematic representation of the proposed role of the DNA-bound pioneer TF PU.1 in the bystander and rapidly upregulated expression of immediate-early stimulus-induced genes in control and *Itgax*Δ*Uqcrq* cDC1s.

Data are presented as mean ± SEM (dots represent individual data points) or paired data points and pooled from at least two independent experiments (A–H and R–U). Statistical analysis by using mixed-effect model with Tukey's multiple comparison test (H) and empirical Bayes-moderated *t* statistics, with *p* values adjusted for multiple testing using the Benjamini-Hochberg method (J) and one-way ANOVA (R and U).

See also Figure S6.

To interrogate this hypothesis, we first assessed the upregulation of co-stimulatory molecules by splenic wild-type and *Aox*^{Rosa26} cDCs treated *ex vivo* with the CIII inhibitors antimycin A or myxothiazol or CIV inhibitor KCN before stimulation with PIC and R848. AOX expression per se did not interfere with the activation of cDCs. Contrary, the decreased expression of CD40 and CD80 by stimulated wild-type cDC1s upon CIII and CIV inhibitor treatment was largely reverted in *Aox*^{Rosa26} cDC1s (Figure S6H). Next, we analyzed the immunogenic activation in splenic cDCs of *Itgax*Δ*Uqcrq Aox*^{Rosa26} mice after stimulation *in vivo*. Overexpression of *Aox* in *Uqcrq*$^{f/f}$ *Aox*^{Rosa26} mice did not affect CD40, CCR7, and CD80 expression in the steady state and their stimulation-induced upregulation in cDC1s and cDC2s, compared with *Uqcrq*$^{f/f}$ control mice. Of note, AOX expression in *Itgax*Δ*Uqcrq Aox*^{Rosa26} cDC1s completely restored the impaired induction of DC activation markers in *Itgax*Δ*Uqcrq* cDC1s *in vivo*. No major alterations were found in cDC2s of any genotype (Figures 4Q–4S and S6I). Consistently, AOX expression also functionally rescued the impaired induction of anti-cancer immunity by *Uqcrq*-deficient cDC1, as vaccinating B16-OVA tumor-bearing mice with stimulated OVA antigen-loaded *Itgax*Δ*Uqcrq Aox*^{Rosa26} cDC1s significantly reduced tumor burden, compared with *Itgax*Δ*Uqcrq* cDC1 treatment, to levels of vaccination with *Uqcrq*$^{f/f}$ cDC1 controls (Figures 4T and 4U).

Overall, these data show that the diminished immunogenic responsiveness of CIII-impaired cDC1s is driven by the decreased electron flow through the ETC, which disrupts redox balance and the availability of TCA cycle-related metabolites. This effect is largely independent of ATP production or the MMP. Instead, an active ETC ensures the timely activation of cDC1s by finely tuning an optimal DNA methylation state of immediate-early stimulus-responsive genes regulated by TFs, such as PU.1 and AP-1 (Figure 4V). Notably, *Uqcrq*-deficient cDC2s show graded metabolic alterations, likely due to their lower OXPHOS engagement and baseline flow of electrons into the ETC, compared with cDC1s.[7]

DISCUSSION

Elevated mitochondrial respiration has been linked to the tolerogenic function of DCs. This association is based on studies inhibiting OXPHOS in cultures of human moDCs[17,18] and on the rapid downregulation of oxygen consumption upon immunogenic stimulation by GMDCs *ex vivo*[11,20] as well as by splenic CD11c$^+$ cells in an interferon alpha receptor (IFNAR)- and HIF1α-dependent manner.[22] However, subsequent studies challenged this notion by showing a higher engagement of OXPHOS in cDC1s vs. cDC2s and functional defects in non-tolerogenic cDCs with dysfunctional mitochondria in the steady state.[7,14,19] Here, we unequivocally demonstrate *in vivo* that the mitochondrial ETC is crucial for the immunogenic responsiveness of cDC1s but less so for cDC2s, and we also unveil the underlying mechanism.

The engagement of mitochondrial respiration upon immunogenic activation differed between cDC subsets. The OCR of mouse cDC2s initially remained unaltered, followed by a decrease after prolonged stimulation, similar to human blood cDC2s[14] and GMDCs.[20] In line, ETC dysfunction mildly affected the metabolic homeostasis of cDC2s and their transcriptome and function. In contrast, cDC1s progressively increased their OCR upon activation. Genetic interference with CIII or CIV partially decreased respiration and strongly compromised the intrinsic immunogenic functions of cDC1s after stimulation *ex vivo* or *in vivo*, namely, upregulation of co-stimulatory molecules, cytokine expression, migration, and CD4$^+$ and CD8$^+$ T cell priming. This was explained by the strongly decreased transcription of immunogenic activation-related genes in both resting and stimulated ETC-impaired cDC1s. Notably, ATP and ROS concentrations were unaffected in cDC1s and cDC2s with dysfunctional mitochondrial respiration. In line, neither glycolysis- nor OXPHOS-derived ATP is essential for immunogenic activation of GMDCs.[11] Those data indicate the great flexibility of activated DCs to meet their bioenergetic demands. Instead, uncoupling electron flow through the ETC from ATP and ROS production by means of AOX expression identified the metabolic dysregulation resulting from ETC blockade as the cause of the immunogenic dysfunction of cDC1s.

CIII-impaired cDC1s accumulated 2-HG concentrations and decreased their NAD$^+$/NADH ratio, which together can inhibit both methylcytosine dioxygenases and histone demethylases. In addition, other essential metabolites for DNA methylation, such as succinate[50] and serine,[47] were dysregulated. In accordance, cDC1s with a dysfunctional CIII exhibited an altered state of DNA methylation that caused the global downregulation of immunogenic gene expression. Interestingly, CIII impairment resulting in DNA hypermethylation and hypomethylation in cDC1s at baseline was rescued by AOX expression, which may be a reflection of complex and rapid DNA methylation dynamics in cDCs, as described during moDC differentiation or upon their bacterial infection.[51,52] DNA methylation can be metabolically controlled by involving serine/one-carbon metabolism,[47] and modulation of the activity of DNA methylases alters the function of differentiated DCs.[53,54] Our data suggest a potential regulation of these processes by the ETC in cDCs, which merits future investigation. Notably, despite these epigenetic and transcriptomic alterations, the expression of genes underlying the cellular identity of CIII-impaired cDC1s and cDC2s remained intact. This is consistent with metabolic and biochemical uncoupling of differentiation and effector functions, as shown by modulation of CII in CD4$^+$ T cells[55] and CIII in CD8$^+$ T cells.[56] The functional activities of regulatory T cells with an impaired CIII are also hampered due to promoter hypermethylation and dysregulation of functional genes, but their presence and differentiation are unaltered.[23] However, how mitochondrial metabolism and TCA cycle metabolites can finely tune the regulation of specific loci in the genome that uniquely regulate specific cell functions remains generally poorly understood.

Notably, we found the enrichment of PU.1 and AP-1 family member binding sites to be a common pattern among the differentially methylated DNA regions in CIII-impaired cDC1s, which were rescued by AOX-mediated re-establishment of electron flow through the ETC. PU.1 is a pioneer TF from the Ets family that controls DC poiesis and function. Complete deletion of PU.1 (in CD11c-expressing cells) in mice leads to decreased numbers, altered identity marker expression, and impaired immunogenic function of cDC1s and cDC2s.[57,58] Downregulation or loss of PU.1 activity in fully differentiated mouse GMDCs or cDCs hampers their capacity for T cell priming and

migration.[32–35] PU.1 binds to thousands of genome regions in differentiated cDCs,[57] and no other studied TF binds to more DNA loci in GMDCs.[37] The AP-1 TF JunB can occupy PU.1 binding sites to set a basal expression and poise these genomic regions for rapid expression upon DC stimulation.[36] In line, JunB is also required for cDC1 differentiation and function.[48] Notably, PU.1 is known to recruit demethylases (e.g., TET2) to its DNA binding sites.[39] Moreover, co-stimulatory molecule expression in human moDCs is decreased upon TET2 inhibition in a PU.1-mediated manner[38] and increased in the presence of ascorbic acid, which increases TET2 activity.[59] We here confirmed that ascorbic acid pre-treatment increased the stimulation-induced upregulation of co-stimulatory molecules by primary mouse cDCs in a TET2-dependent manner. Current models propose that stimuli-induced gene overexpression precedes DNA demethylation (e.g., by TET2 recruitment).[45,60] Yet our data suggest that enzymes in charge of DNA (de-) methylation, including TET2, are also involved in the TF ensemble that regulates rapid DC responses to stimuli and that their activity is controlled by OXPHOS metabolism.

Thus, we propose a layer of graded regulation of cDC1 and cDC2 function that mainly mediates the rapid immunogenic responsiveness of cDC1s upon activation. The highly active ETC maintains a fine metabolic balance in cDC1s, which facilitates optimal DNA methylation of PU.1 and AP-1 binding regions already in unstimulated cells. This results in a bystander expression of immediate-early stimulus-inducible genes in the steady state, which can be rapidly induced in cDC1s upon immunogenic stimulation and are thus poised for activation. Accordingly, we found that CIII-impaired cDC1s showed a delayed and hampered upregulation of the expression of immunogenic activation-associated genes when stimulated, compared with control cDC1s. Importantly, the genes that were significantly downregulated in CIII-impaired cDC1s in the steady state (bystander expression) mostly correspond to genes that were upregulated in cDC1s shortly after activation (immediate-early stimulus-inducible genes). Linking individual genes within this program to specific functional deficits of CIII-impaired cDC1s, such as aspects of T cell priming or migration, will require a dedicated mechanistic study. Yet overall, we show that this altered mitochondrial-epigenetic balance translates into a globally faulty immunogenic function of cDC1s with a dysfunctional CIII.

On the other hand, the flow of electrons through the ETC is generally lower in splenic cDC2s than cDC1s in the steady state,[7] and we observed a further decrease in OXPHOS activity in activated compared with resting cDC2s. This in turn yielded cDC2s less vulnerable for CIII downregulation, as we found no major metabolic or epigenetic alterations upon CIII impairment. Moreover, their mildly dysregulated immunogenic activation-associated gene expression was fully recovered upon stimulation, which explains the mildly impaired functionality of cDC2s with a dysfunctional CIII. Nevertheless, complete blockade of CIII activity using inhibitors, or global *Tet2* deletion, similarly affected functional features of cDC1s and cDC2s. As TET2 loss also hampers the immunogenic activation of human moDCs,[38] our data suggest that the ETC provides a nuanced layer of regulation upstream of DNA methylation, which varies across DC subtypes and merits further investigation.

This study reveals a metabolic mechanism that regulates the immunogenic responsiveness of cDC subsets in a graded manner, which may provide innovative strategies to tailor DC function.

Limitations of the study

Here, we uncovered a gene expression program regulated by ETC/OXPHOS activity that operates independently of ATP generation. Mechanistically, we focused on the ETC-mediated control of metabolic balance and DNA methylation status via α-KG-dependent methylcytosine dioxygenases such as TET2, which regulate the rapid immunogenic function of cDC1s. Yet the specific regulation of the functionality of different cDC subsets by TET2 per se requires additional research efforts. Additionally, our observation that CIII impairment leads to DNA hypomethylation alongside reduced gene expression highlights the locus-specific and still incompletely understood relationship between DNA methylation and transcriptional regulation,[61,62] which merits a dedicated study. Moreover, while we show a number of genes whose expression is largely impacted by CIII deficiency in steady-state cDC1s and link this to lower immunogenicity and T cell activation, the specific contribution and regulation of particular genes require further mechanistic study. Nevertheless, we propose that ectopic AOX expression or pharmacological activation of TET2 in cDCs may represent promising therapeutic strategies to boost cDC1 immunogenicity.

RESOURCE AVAILABILITY

Lead contact

Requests for further information and resources should be directed to and will be fulfilled by the lead contact, David Sancho (dsancho@cnic.es).

Materials availability

This study did not generate new, unique reagents.

Data and code availability

The RNA-seq , ATAC-seq , DNA methylation array , and WGBS data that were generated in this study have been deposited at GEO (GEO: GSE276024, GSE276020, GSE276025, and GSE308685, respectively). Code used for the analysis of bulk RNA-seq, ATAC-seq, DNA methylation array, and metabolomics has been deposited at GitHub (https://github.com/DSanchoLab/Heras-Murillo_cDC1-ETC_2025). Any additional information required to reanalyze the data reported in this paper is available from the lead contact upon request.

ACKNOWLEDGMENTS

We thank the members of the D.S. and S.K.W. laboratories and the laboratory of Salvador Iborra for discussions and critical reading of the manuscript. We thank the staff at the CNIC technical units, especially the Animal, Cellomics, and Genomics facilities, for technical support. This project was supported by the "la Caixa" Foundation (ID 100010434) INPhINIT Fellowship code LCF/BQ/IN17/11620074 (I.H.-M.). I.M. lab work was supported by Fundación Fero. P.H.-A. is supported by RYC2022-036516-I. Work in the D.S. laboratory received support from the CNIC; Ministerio de Ciencia, Innovación y Universidades (MICIU) PID2022-137712OB-I00, PDC2025-165319-I00, CPP2022-009762, and CPP2024-011365 MICIU/AEI/10.13039/501100011033 Agencia Estatal de Investigación, Unión Europea NextGenerationEU/PRTR; Comunidad de Madrid (P2022/BMD-7333 INMUNOVAR-CM); Scientific Foundation of the Spanish Association Against Cancer (AECC-PRYGN246642SANC); Worldwide Cancer Research WWCR-25-0080; European Union ERC-POC-2023-GA-101158245-ImnovAth; research agreement with Inmunotek S.L.; Fundación CRIS contra el cáncer (excellence2025_03); and "la Caixa" Foundation (LCF/PR/HR23/52430012 and

LCF/PR/HR22/52420019). The S.K.W. laboratory and this work are supported by the IRB Barcelona, the European Union, and European Research Council's Horizon Europe programme (ERC-2023-StG "MyTissue" project number 101117470) and by grants RYC2022-036400-I and PID2022-140715OA-I00 from MCIN/AEI/10.13039/501100011033 Agencia Estatal de Investigación, Unión Europea NextGenerationEU/PRTR. IRB Barcelona receives institutional funding from the Spanish Ministry of Science and Innovation, through the Centres of Excellence Severo Ochoa Award, and from the CERCA Programme/Generalitat de Catalunya. M.A.Z. and J.J.F. were supported by "la Caixa" Foundation under the project code LCF/PR/HR22/52420011 and by Fundació "La Marató TV3" (grant 202314-31). J.A.E. is supported by PID2024-158440OB-100, TED2024-158440OB-I00, and PID2021-127988OB-100, funded by MICIU/AEI/10.13039/501100011033 and the European Union "NextGenerationEU"/Plan de Recuperación Transformación y Resiliencia/PRTR; CIBERFES (CB16/10/00282); Fundación "la Caixa" (LCF/PR/HR23/52430010); and ERC-2024-ADG (GA 101198761). N.S.C. was funded by 5R01CA290678. The CNIC is supported by the Instituto de Salud Carlos III (ISCIII), the MICIU, and the Pro CNIC Foundation and is a Severo Ochoa Center of Excellence (CEX2020-001041-S funded by MICIU/AEI/10.13039/501100011033).

AUTHOR CONTRIBUTIONS

I.H.-M., S.K.W., and D.S. conceptualized the study, designed the experiments, and wrote the manuscript. I.H.-M. and S.K.W. performed experiments and analyzed most of the data. A.B.G., C.B.-E., P.M., A.M., and S.M.-C. helped with experimental procedures. I.H.-M., D.M., and J.C.-S. carried out the bioinformatics analysis. S.K.W. and D.S. supervised the research. J.C.-S., P.H.-A., and E.B. helped with data interpretation. M.A.Z., J.J.F., M.S., I.M., J.A.E., and N.S.C. provided essential material.

DECLARATION OF INTERESTS

S.K.W. serves as a consultant for ONA therapeutics (Barcelona, Spain). I.M. reports grant funding from Roche, BMS, AstraZeneca, Genmab, and Catalym and advisory roles with AstraZeneca, Roche, BMS, Catalym, Genmab, Pioneers, Pharmamar, F-Star, Invox, Biontech, Highlight Therapeutics, Servier, Pierre Fabre, Bright Peaks, and Alligator.

DECLARATION OF GENERATIVE AI AND AI-ASSISTED TECHNOLOGIES IN THE WRITING PROCESS

During the preparation of this work the authors used M365 Copilot to refine language and improve clarity in the text. After using this tool, the authors reviewed and edited the content as needed and take full responsibility for the content of the publication.

STAR★METHODS

Detailed methods are provided in the online version of this paper and include the following:

SUPPLEMENTAL INFORMATION

Supplemental information can be found online at https://doi.org/10.1016/j.cmet.2026.03.012.

Received: September 17, 2024
Revised: December 2, 2025
Accepted: March 20, 2026
Published: April 15, 2026

REFERENCES

1. Cabeza-Cabrerizo, M., Cardoso, A., Minutti, C.M., Pereira Da Costa, M., and Reis e Sousa, C. (2021). Dendritic cells revisited. Annu. Rev. Immunol. *39*, 131–166. https://doi.org/10.1146/annurev-immunol-061020-053707.
2. Heras-Murillo, I., Adán-Barrientos, I., Galán, M., Wculek, S.K., and Sancho, D. (2024). Dendritic cells as orchestrators of anticancer immunity and immunotherapy. Nat. Rev. Clin. Oncol. *21*, 257–277. https://doi.org/10.1038/s41571-024-00859-1.
3. Wculek, S.K., Khouili, S.C., Priego, E., Heras-Murillo, I., and Sancho, D. (2019). Metabolic control of dendritic cell functions: digesting information. Front. Immunol. *10*, 775. https://doi.org/10.3389/fimmu.2019.00775.
4. Minarrieta, L., Velasquez, L.N., Sparwasser, T., and Berod, L. (2021). Dendritic cell metabolism: moving beyond in vitro-culture-generated paradigms. Curr. Opin. Biotechnol. *68*, 202–212. https://doi.org/10.1016/j.copbio.2020.12.010.
5. Møller, S.H., Wang, L., and Ho, P.-C. (2022). Metabolic programming in dendritic cells tailors immune responses and homeostasis. Cell. Mol. Immunol. *19*, 370–383. https://doi.org/10.1038/s41423-021-00753-1.
6. Martínez-Reyes, I., and Chandel, N.S. (2020). Mitochondrial TCA cycle metabolites control physiology and disease. Nat. Commun. *11*, 102. https://doi.org/10.1038/s41467-019-13668-3.
7. Du, X., Wen, J., Wang, Y., Karmaus, P.W.F., Khatamian, A., Tan, H., Li, Y., Guy, C., Nguyen, T.M., Dhungana, Y., et al. (2018). Hippo/Mst signalling couples metabolic state and immune function of CD8α+ dendritic cells. Nature *558*, 141–145. https://doi.org/10.1038/s41586-018-0177-0.
8. Kratchmarov, R., Viragova, S., Kim, M.J., Rothman, N.J., Liu, K., Reizis, B., and Reiner, S.L. (2018). Metabolic control of cell fate bifurcations in a hematopoietic progenitor population. Immunol. Cell Biol. *96*, 863–871. https://doi.org/10.1111/imcb.12040.
9. Argüello, R.J., Combes, A.J., Char, R., Gigan, J.-P., Baaziz, A.I., Bousiquot, E., Camosseto, V., Samad, B., Tsui, J., Yan, P., et al. (2020). SCENITH: a flow cytometry-based method to functionally profile energy metabolism with single-cell resolution. Cell Metab. *32*, 1063–1075.e7. https://doi.org/10.1016/j.cmet.2020.11.007.
10. Adamik, J., Munson, P.V., Hartmann, F.J., Combes, A.J., Pierre, P., Krummel, M.F., Bendall, S.C., Argüello, R.J., and Butterfield, L.H. (2022). Distinct metabolic states guide maturation of inflammatory and tolerogenic dendritic cells. Nat. Commun. *13*, 5184. https://doi.org/10.1038/s41467-022-32849-1.
11. Everts, B., Amiel, E., Huang, S.C.-C., Smith, A.M., Chang, C.-H., Lam, W.Y., Redmann, V., Freitas, T.C., Blagih, J., van der Windt, G.J.W., et al. (2014). TLR-driven early glycolytic reprogramming via the kinases TBK1-IKKε supports the anabolic demands of dendritic cell activation. Nat. Immunol. *15*, 323–332. https://doi.org/10.1038/ni.2833.

12. Hansen, I.S., Krabbendam, L., Bernink, J.H., Loayza-Puch, F., Hoepel, W., Van Burgsteden, J.A., Kuijper, E.C., Buskens, C.J., Bemelman, W.A., Zaat, S.A.J., et al. (2018). FcαRI co-stimulation converts human intestinal CD103+ dendritic cells into pro-inflammatory cells through glycolytic reprogramming. Nat. Commun. *9*, 863. https://doi.org/10.1038/s41467-018-03318-5.

13. Guak, H., Al Habyan, S., Ma, E.H., Aldossary, H., Al-Masri, M., Won, S.Y., Ying, T., Fixman, E.D., Jones, R.G., McCaffrey, L.M., et al. (2018). Glycolytic metabolism is essential for CCR7 oligomerization and dendritic cell migration. Nat. Commun. *9*, 2463. https://doi.org/10.1038/s41467-018-04804-6.

14. Basit, F., Mathan, T., Sancho, D., and de Vries, I.J.M. (2018). Human dendritic cell subsets undergo distinct metabolic reprogramming for immune response. Front. Immunol. *9*, 2489. https://doi.org/10.3389/fimmu.2018.02489.

15. Liu, J., Zhang, X., Chen, K., Cheng, Y., Liu, S., Xia, M., Chen, Y., Zhu, H., Li, Z., and Cao, X. (2019). CCR7 chemokine receptor-inducible lnc-Dpf3 restrains dendritic cell migration by inhibiting HIF-1α-mediated glycolysis. Immunity *50*, 600–615.e15. https://doi.org/10.1016/j.immuni.2019.01.021.

16. Lawless, S.J., Kedia-Mehta, N., Walls, J.F., McGarrigle, R., Convery, O., Sinclair, L.V., Navarro, M.N., Murray, J., and Finlay, D.K. (2017). Glucose represses dendritic cell-induced T cell responses. Nat. Commun. *8*, 15620. https://doi.org/10.1038/ncomms15620.

17. Malinarich, F., Duan, K., Hamid, R.A., Bijin, A., Lin, W.X., Poidinger, M., Fairhurst, A.-M., and Connolly, J.E. (2015). High mitochondrial respiration and glycolytic capacity represent a metabolic phenotype of human tolerogenic dendritic cells. J. Immunol. *194*, 5174–5186. https://doi.org/10.4049/jimmunol.1303316.

18. Ferreira, G.B., Vanherwegen, A.S., Eelen, G., Gutiérrez, A.C.F., Van Lommel, L., Marchal, K., Verlinden, L., Verstuyf, A., Nogueira, T., Georgiadou, M., et al. (2015). Vitamin D3 induces tolerance in human dendritic cells by activation of intracellular metabolic pathways. Cell Rep. *10*, 711–725. https://doi.org/10.1016/j.celrep.2015.01.013.

19. Chougnet, C.A., Thacker, R.I., Shehata, H.M., Hennies, C.M., Lehn, M.A., Lages, C.S., and Janssen, E.M. (2015). Loss of phagocytic and antigen cross-presenting capacity in aging dendritic cells is associated with mitochondrial dysfunction. J. Immunol. *195*, 2624–2632. https://doi.org/10.4049/jimmunol.1501006.

20. Everts, B., Amiel, E., Van Der Windt, G.J.W., Freitas, T.C., Chott, R., Yarasheski, K.E., Pearce, E.L., and Pearce, E.J. (2012). Commitment to glycolysis sustains survival of NO-producing inflammatory dendritic cells. Blood *120*, 1422–1431. https://doi.org/10.1182/blood-2012-03-419747.

21. Yoshida, H., Lareau, C.A., Ramirez, R.N., Rose, S.A., Maier, B., Wroblewska, A., Desland, F., Chudnovskiy, A., Mortha, A., Dominguez, C., et al. (2019). The cis-regulatory atlas of the mouse immune system. Cell *176*, 897–912.e20. https://doi.org/10.1016/j.cell.2018.12.036.

22. Pantel, A., Teixeira, A., Haddad, E., Wood, E.G., Steinman, R.M., and Longhi, M.P. (2014). Direct type I IFN but not MDA5/TLR3 activation of dendritic cells is required for maturation and metabolic shift to glycolysis after poly IC stimulation. PLoS Biol. *12*, e1001759. https://doi.org/10.1371/journal.pbio.1001759.

23. Weinberg, S.E., Singer, B.D., Steinert, E.M., Martinez, C.A., Mehta, M.M., Martínez-Reyes, I., Gao, P., Helmin, K.A., Abdala-Valencia, H., Sena, L.A., et al. (2019). Mitochondrial complex III is essential for suppressive function of regulatory T cells. Nature *565*, 495–499. https://doi.org/10.1038/s41586-018-0846-z.

24. Caton, M.L., Smith-Raska, M.R., and Reizis, B. (2007). Notch–RBP-J signaling controls the homeostasis of CD8- dendritic cells in the spleen. J. Exp. Med. *204*, 1653–1664. https://doi.org/10.1084/jem.20062648.

25. Diaz, F., Thomas, C.K., Garcia, S., Hernandez, D., and Moraes, C.T. (2005). Mice lacking COX10 in skeletal muscle recapitulate the phenotype of progressive mitochondrial myopathies associated with cytochrome c oxidase deficiency. Hum. Mol. Genet. *14*, 2737–2748. https://doi.org/10.1093/hmg/ddi307.

26. Clatworthy, M.R., Aronin, C.E.P., Mathews, R.J., Morgan, N.Y., Smith, K.G.C., and Germain, R.N. (2014). Immune complexes stimulate CCR7-dependent dendritic cell migration to lymph nodes. Nat. Med. *20*, 1458–1463. https://doi.org/10.1038/nm.3709.

27. Rizzitelli, A., Hawkins, E., Todd, H., Hodgkin, P.D., and Shortman, K. (2006). The proliferative response of CD4 T cells to steady-state CD8+ dendritic cells is restricted by post-activation death. Int. Immunol. *18*, 415–423. https://doi.org/10.1093/intimm/dxh382.

28. Wculek, S.K., Amores-Iniesta, J., Conde-Garrosa, R., Khouili, S.C., Melero, I., and Sancho, D. (2019). Effective cancer immunotherapy by natural mouse conventional type-1 dendritic cells bearing dead tumor antigen. J. Immunother. Cancer *7*, 100. https://doi.org/10.1186/s40425-019-0565-5.

29. Robertson, H., Li, J., Kim, H.J., Rhodes, J.W., Harman, A.N., Patrick, E., and Rogers, N.M. (2021). Transcriptomic analysis identifies a tolerogenic dendritic cell signature. Front. Immunol. *12*, 733231. https://doi.org/10.3389/fimmu.2021.733231.

30. Miller, J.C., Brown, B.D., Shay, T., Gautier, E.L., Jojic, V., Cohain, A., Pandey, G., Leboeuf, M., Elpek, K.G., Helft, J., et al. (2012). Deciphering the transcriptional network of the dendritic cell lineage. Nat. Immunol. *13*, 888–899. https://doi.org/10.1038/ni.2370.

31. Buenrostro, J.D., Giresi, P.G., Zaba, L.C., Chang, H.Y., and Greenleaf, W.J. (2013). Transposition of native chromatin for fast and sensitive epigenomic profiling of open chromatin, DNA-binding proteins and nucleosome position. Nat. Methods *10*, 1213–1218. https://doi.org/10.1038/nmeth.2688.

32. Yashiro, T., Takeuchi, H., Nakamura, S., Tanabe, A., Hara, M., Uchida, K., Okumura, K., Kasakura, K., and Nishiyama, C. (2019). PU.1 plays a pivotal role in dendritic cell migration from the periphery to secondary lymphoid organs *via* regulating CCR7 expression. FASEB J. *33*, 11481–11491. https://doi.org/10.1096/fj.201900379RR.

33. Kanada, S., Nishiyama, C., Nakano, N., Suzuki, R., Maeda, K., Hara, M., Kitamura, N., Ogawa, H., and Okumura, K. (2011). Critical role of transcription factor PU.1 in the expression of CD80 and CD86 on dendritic cells. Blood *117*, 2211–2222. https://doi.org/10.1182/blood-2010-06-291898.

34. Yashiro, T., Hara, M., Ogawa, H., Okumura, K., and Nishiyama, C. (2016). Critical role of transcription factor PU.1 in the function of the OX40L/TNFSF4 promoter in dendritic cells. Sci. Rep. *6*, 34825. https://doi.org/10.1038/srep34825.

35. Kitamura, N., Yokoyama, H., Yashiro, T., Nakano, N., Nishiyama, M., Kanada, S., Fukai, T., Hara, M., Ikeda, S., Ogawa, H., et al. (2012). Role of PU.1 in MHC class II expression through transcriptional regulation of class II transactivator pI in dendritic cells. J. Allergy Clin. Immunol. *129*, 814–824.e6. https://doi.org/10.1016/j.jaci.2011.10.019.

36. Paul, F., and Amit, I. (2014). Plasticity in the transcriptional and epigenetic circuits regulating dendritic cell lineage specification and function. Curr. Opin. Immunol. *30*, 1–8. https://doi.org/10.1016/j.coi.2014.04.004.

37. Garber, M., Yosef, N., Goren, A., Raychowdhury, R., Thielke, A., Guttman, M., Robinson, J., Minie, B., Chevrier, N., Itzhaki, Z., et al. (2012). A high-throughput chromatin immunoprecipitation approach reveals principles of dynamic gene regulation in mammals. Mol. Cell *47*, 810–822. https://doi.org/10.1016/j.molcel.2012.07.030.

38. Vento-Tormo, R., Company, C., Rodríguez-Ubreva, J., de la Rica, L., Urquiza, J.M., Javierre, B.M., Sabarinathan, R., Luque, A., Esteller, M., Aran, J.M., et al. (2016). IL-4 orchestrates STAT6-mediated DNA demethylation leading to dendritic cell differentiation. Genome Biol. *17*, 4. https://doi.org/10.1186/s13059-015-0863-2.

39. de la Rica, L., Rodríguez-Ubreva, J., García, M., Islam, A.B.M.M.K., Urquiza, J.M., Hernando, H., Christensen, J., Helin, K., Gómez-Vaquero, C., and Ballestar, E. (2013). PU.1 target genes undergo Tet2-coupled demethylation and DNMT3b-mediated methylation in monocyte-to-osteoclast differentiation. Genome Biol. *14*, R99. https://doi.org/10.1186/gb-2013-14-9-r99.

40. Yue, X., and Rao, A. (2020). TET family dioxygenases and the TET activator vitamin C in immune responses and cancer. Blood *136*, 1394–1401. https://doi.org/10.1182/blood.2019004158.

41. Wu, Q., and Ni, X. (2015). ROS-mediated DNA methylation pattern alterations in carcinogenesis. Curr. Drug Targets *16*, 13–19. https://doi.org/10.2174/1389450116666150113121054.

42. Appleby, R.D., Porteous, W.K., Hughes, G., James, A.M., Shannon, D., Wei, Y.H., and Murphy, M.P. (1999). Quantitation and origin of the mitochondrial membrane potential in human cells lacking mitochondrial DNA. Eur. J. Biochem. *262*, 108–116. https://doi.org/10.1046/j.1432-1327.1999.00350.x.

43. Chakrabarty, R.P., and Chandel, N.S. (2021). Mitochondria as signaling organelles control mammalian stem cell fate. Cell Stem Cell *28*, 394–408. https://doi.org/10.1016/j.stem.2021.02.011.

44. Szibor, M., Dhandapani, P.K., Dufour, E., Holmström, K.M., Zhuang, Y., Salwig, I., Wittig, I., Heidler, J., Gizatullina, Z., Gainutdinov, T., et al. (2017). Broad AOX expression in a genetically tractable mouse model does not disturb normal physiology. Dis. Model. Mech. *10*, 163–171. https://doi.org/10.1242/dmm.027839.

45. Chen, L.-L., Morcelle, C., Cheng, Z.-L., Chen, X., Xu, Y., Gao, Y., Song, J., Li, Z., Smith, M.D., Shi, M., et al. (2022). Itaconate inhibits TET DNA dioxygenases to dampen inflammatory responses. Nat. Cell Biol. *24*, 353–363. https://doi.org/10.1038/s41556-022-00853-8.

46. Xiao, M., Yang, H., Xu, W., Ma, S., Lin, H., Zhu, H., Liu, L., Liu, Y., Yang, C., Xu, Y., et al. (2012). Inhibition of α-KG-dependent histone and DNA demethylases by fumarate and succinate that are accumulated in mutations of FH and SDH tumor suppressors. Genes Dev. *26*, 1326–1338. https://doi.org/10.1101/gad.191056.112.

47. Maddocks, O.D.K., Labuschagne, C.F., Adams, P.D., and Vousden, K.H. (2016). Serine metabolism supports the methionine cycle and DNA/RNA methylation through de novo ATP synthesis in cancer cells. Mol. Cell *61*, 210–221. https://doi.org/10.1016/j.molcel.2015.12.014.

48. Novoszel, P., Drobits, B., Holcmann, M., Fernandes, C.S., Tschismarov, R., Derdak, S., Decker, T., Wagner, E.F., and Sibilia, M. (2021). The AP-1 transcription factors c-Jun and JunB are essential for CD8α conventional dendritic cell identity. Cell Death Differ. *28*, 2404–2420. https://doi.org/10.1038/s41418-021-00765-4.

49. Dunand-Sauthier, I., Santiago-Raber, M.-L., Capponi, L., Vejnar, C.E., Schaad, O., Irla, M., Seguín-Estévez, Q., Descombes, P., Zdobnov, E.M., Acha-Orbea, H., et al. (2011). Silencing of c-Fos expression by microRNA-155 is critical for dendritic cell maturation and function. Blood *117*, 4490–4500. https://doi.org/10.1182/blood-2010-09-308064.

50. Xu, W., Yang, H., Liu, Y., Yang, Y., Wang, P., Kim, S.-H., Ito, S., Yang, C., Wang, P., Xiao, M.-T., et al. (2011). Oncometabolite 2-hydroxyglutarate is a competitive inhibitor of α-ketoglutarate-dependent dioxygenases. Cancer Cell *19*, 17–30. https://doi.org/10.1016/j.ccr.2010.12.014.

51. Zhang, X., Ulm, A., Somineni, H.K., Oh, S., Weirauch, M.T., Zhang, H.-X., Chen, X., Lehn, M.A., Janssen, E.M., and Ji, H. (2014). DNA methylation dynamics during ex vivo differentiation and maturation of human dendritic cells. Epigenetics Chromatin *7*, 21. https://doi.org/10.1186/1756-8935-7-21.

52. Pacis, A., Tailleux, L., Morin, A.M., Lambourne, J., MacIsaac, J.L., Yotova, V., Dumaine, A., Danckaert, A., Luca, F., Grenier, J.-C., et al. (2015). Bacterial infection remodels the DNA methylation landscape of human dendritic cells. Genome Res. *25*, 1801–1811. https://doi.org/10.1101/gr.192005.115.

53. Xue, J., Wu, Y., Liu, Z., Duan, S., Ji, Y., Dong, R., Lu, L., Guan, F., Geng, Z., Li, Y., et al. (2025). Epigenetic reprogramming of dendritic cells by DNMT1 inhibition attenuates Th2 skewing in allergic airway inflammation. Cell Commun. Signal. *23*, 459. https://doi.org/10.1186/s12964-025-02467-7.

54. Huang, D., Tang, B., Li, Q., Tong, B., and Liu, N. (2025). Role of DNMT3a expression and nuclear translocation under ELAVL1 mediation for dendritic cell function and Th17/Treg balance in COPD. Transl. Res. *279*, 1–15. https://doi.org/10.1016/j.trsl.2025.03.002.

55. Bailis, W., Shyer, J.A., Zhao, J., Canaveras, J.C.G., Al Khazal, F.J., Qu, R., Steach, H.R., Bielecki, P., Khan, O., Jackson, R., et al. (2019). Distinct modes of mitochondrial metabolism uncouple T cell differentiation and function. Nature *571*, 403–407. https://doi.org/10.1038/s41586-019-1311-3.

56. Steinert, E.M., Furtado Bruza, B., Danchine, V.D., Grant, R.A., Vasan, K., Kharel, A., Zhang, Y., Cui, W., Szibor, M., Weinberg, S.E., et al. (2025). Mitochondrial respiration is necessary for CD8+ T cell proliferation and cell fate. Nat. Immunol. *26*, 1267–1274. https://doi.org/10.1038/s41590-025-02202-x.

57. Chopin, M., Lun, A.T., Zhan, Y., Schreuder, J., Coughlan, H., D'Amico, A., Mielke, L.A., Almeida, F.F., Kueh, A.J., Dickins, R.A., et al. (2019). Transcription factor PU.1 promotes conventional dendritic cell identity and function via induction of transcriptional regulator DC-SCRIPT. Immunity *50*, 77–90.e5. https://doi.org/10.1016/j.immuni.2018.11.010.

58. Carotta, S., Dakic, A., D'Amico, A., Pang, S.H.M., Greig, K.T., Nutt, S.L., and Wu, L. (2010). The transcription factor PU.1 controls dendritic cell development and Flt3 cytokine receptor expression in a dose-dependent manner. Immunity *32*, 628–641. https://doi.org/10.1016/j.immuni.2010.05.005.

59. Morante-Palacios, O., Godoy-Tena, G., Calafell-Segura, J., Ciudad, L., Martínez-Cáceres, E.M., Sardina, J.L., and Ballestar, E. (2022). Vitamin C enhances NF-κB-driven epigenomic reprogramming and boosts the immunogenic properties of dendritic cells. Nucleic Acids Res. *50*, 10981–10994. https://doi.org/10.1093/nar/gkac941.

60. Pacis, A., Mailhot-Léonard, F., Tailleux, L., Randolph, H.E., Yotova, V., Dumaine, A., Grenier, J.-C., and Barreiro, L.B. (2019). Gene activation precedes DNA demethylation in response to infection in human dendritic cells. Proc. Natl. Acad. Sci. USA *116*, 6938–6943. https://doi.org/10.1073/pnas.1814700116.

61. Jones, P.A. (2012). Functions of DNA methylation: islands, start sites, gene bodies and beyond. Nat. Rev. Genet. *13*, 484–492. https://doi.org/10.1038/nrg3230.

62. Dhar, G.A., Saha, S., Mitra, P., and Nag Chaudhuri, R. (2021). DNA methylation and regulation of gene expression: Guardian of our health. Nucleus *64*, 259–270. https://doi.org/10.1007/s13237-021-00367-y.

63. Fuster, J.J., Zuriaga, M.A., Zorita, V., MacLauchlan, S., Polackal, M.N., Viana-Huete, V., Ferrer-Pérez, A., Matesanz, N., Herrero-Cervera, A., Sano, S., et al. (2020). TET2-loss-of-function-driven clonal hematopoiesis exacerbates experimental insulin resistance in aging and obesity. Cell Rep. *33*, 108326. https://doi.org/10.1016/j.celrep.2020.108326.

64. Aryee, M.J., Jaffe, A.E., Corrada-Bravo, H., Ladd-Acosta, C., Feinberg, A.P., Hansen, K.D., and Irizarry, R.A. (2014). Minfi: a flexible and comprehensive Bioconductor package for the analysis of Infinium DNA methylation microarrays. Bioinformatics *30*, 1363–1369. https://doi.org/10.1093/bioinformatics/btu049.

65. Sánchez-Paulete, A.R., Cueto, F.J., Martínez-López, M., Labiano, S., Morales-Kastresana, A., Rodríguez-Ruiz, M.E., Jure-Kunkel, M., Azpilikueta, A., Aznar, M.A., Quetglas, J.I., et al. (2016). Cancer immunotherapy with immunomodulatory anti-CD137 and anti–PD-1 monoclonal antibodies requires BATF3-dependent dendritic cells. Cancer Discov. *6*, 71–79. https://doi.org/10.1158/2159-8290.CD-15-0510.

66. Carvalho, B.S., and Irizarry, R.A. (2010). A framework for oligonucleotide microarray preprocessing. Bioinformatics *26*, 2363–2367. https://doi.org/10.1093/bioinformatics/btq431.

67. Naik, S.H., Proietto, A.I., Wilson, N.S., Dakic, A., Schnorrer, P., Fuchsberger, M., Lahoud, M.H., O'Keeffe, M., Shao, Q.X., Chen, W.F., et al. (2005). Cutting edge: generation of splenic CD8+ and CD8- dendritic cell equivalents in Fms-like tyrosine kinase 3 ligand bone marrow cultures. J. Immunol. *174*, 6592–6597. https://doi.org/10.4049/jimmunol.174.11.6592.

68. Wittig, I., Braun, H.-P., and Schägger, H. (2006). Blue native PAGE. Nat. Protoc. *1*, 418–428. https://doi.org/10.1038/nprot.2006.62.

69. Krämer, A., Green, J., Pollard, J., and Tugendreich, S. (2014). Causal analysis approaches in Ingenuity Pathway Analysis. Bioinformatics *30*, 523–530. https://doi.org/10.1093/bioinformatics/btt703.

70. Amemiya, H.M., Kundaje, A., and Boyle, A.P. (2019). The ENCODE blacklist: identification of problematic regions of the genome. Sci. Rep. *9*, 9354. https://doi.org/10.1038/s41598-019-45839-z.

71. Robinson, M.D., McCarthy, D.J., and Smyth, G.K. (2010). edgeR: a Bioconductor package for differential expression analysis of digital gene

expression data. Bioinformatics *26*, 139–140. https://doi.org/10.1093/bioinformatics/btp616.

72. Morante-Palacios, O., and Ballestar, E. (2021). shinyÉPICo: a graphical pipeline to analyze Illumina DNA methylation arrays. Bioinformatics *37*, 257–259. https://doi.org/10.1093/bioinformatics/btaa1095.

73. Heinz, S., Benner, C., Spann, N., Bertolino, E., Lin, Y.C., Laslo, P., Cheng, J.X., Murre, C., Singh, H., and Glass, C.K. (2010). Simple combinations of lineage-determining transcription factors prime cis-regulatory elements required for macrophage and B cell identities. Mol. Cell *38*, 576–589. https://doi.org/10.1016/j.molcel.2010.05.004.

STAR★METHODS

KEY RESOURCES TABLE

REAGENT or RESOURCE	SOURCE	IDENTIFIER
Antibodies		
anti-mouse CD16/CD32, clone 2.4G2	Tonbo Biosciences	Cat# 70-0161; RRID: AB_2621487
anti-mouse CD45.1, clone A20	eBioscience	Cat# 17-0453-82; RRID: AB_469398
anti-mouse CD44, clone IM7	eBioscience	Cat# 11-0441-82; RRID: AB_465045
anti-mouse CD62L, clone MEL-14	eBioscience	Cat# 12-0621-82; RRID: AB_465721
anti-mouse CD8, clone 53-6.7	BD Biosciences	Cat# 561967; RRID: AB_396769
anti-mouse CD11b, clone M1/70	BD Biosciences	Cat# 561098; RRID: AB_394491
anti-mouse I-A/I-E (MHC-II), clone 2G9	BD Biosciences	Cat# 562009; RRID: AB_394958
anti-mouse SIRPα, clone P84	BD Biosciences	Cat# 770060; RRID: AB_3691930
anti-mouse CD40, clone 3/23	BD Biosciences	Cat# 558695; RRID: AB_1645224
anti-mouse CD3, clone 17A2	BD Biosciences	Cat# 565643; RRID: AB_2739319
anti-mouse CD11c, clone N418	BioLegend	Cat# 117352; RRID: AB_2572124
anti-mouse XCR1, clone ZET	BioLegend	Cat# 148204; RRID: AB_2563843
anti-mouse B220, clone C363-16A	BioLegend	Cat# 103202; RRID: AB_312987
anti-mouse CD80, clone 16-10A1	BioLegend	Cat# 104714; RRID: AB_313135
anti-mouse CD45.2, clone 104	BioLegend	Cat# 109808; RRID: AB_313445
anti-mouse CD90, clone 53-2.1	BioLegend	Cat# 140312; RRID: AB_10640728
anti-mouse CCR3, clone J073E5	BioLegend	Cat# 144506; RRID: AB_2561534
anti-mouse CCR7, clone 4B12	BioLegend	Cat# 120124; RRID: AB_2616688
anti-mouse OX40L, clone RM134L	BioLegend	Cat# 108814; RRID: AB_2565745
anti-mouse PDL1, clone 10F.962	BioLegend	Cat# 155404; RRID: AB_2728223
anti-mouse CD19, clone 6D5	BioLegend	Cat# 115506; RRID: AB_313641
anti-mouse CD24, clone M1/69	BioLegend	Cat# 114308; RRID: AB_3083267
anti-mouse B220, clone RA3-6B2	BioLegend	Cat# 103208; RRID: AB_312993
anti-mouse H-2Kb/H-2Db (MHC-I), clone 28-8-6	BioLegend	Cat# 114608; RRID: AB_313599
anti-mouse CD86, clone GL1	ThermoFisher	Cat# PE-65068; RRID: AB_2883865
anti-mouse FOXP3, clone FJK-16s	Invitrogen	Cat# 11-5773-82; RRID: AB_465243
anti-mouse CD25, clone PC61.5	Tonbo Biosciences	Cat# 50-0251; RRID: AB_2621757
anti-mouse IFNγ antibody, clone XMG1.2	BioLegend	Cat# 505826; RRID: AB_2295770
anti-human CD141, clone AD5-14H12	Miltenyi Biotec	Cat# 130-113-317; RRID: AB_2751167
anti-human CD1c, clone L161	BioLegend	Cat# 331502; RRID: AB_1088995
anti-human HLA-DR, clone L243	BioLegend	Cat# 307634; RRID: AB_3106101
anti-human CD80, clone 2D10	BioLegend	Cat# 305208; RRID: AB_314504
anti-human CD86, clone 2331(FUN-1)	BD Biosciences	Cat# 555655; RRID: AB_396010
anti-NDUFA9, clone 20C11B11B11	Invitrogen	Cat# 459100; RRID: AB_10376187
anti-SDHA, clone 2E3GC12FB2AE2	Invitrogen	Cat# 459200; RRID: AB_10838019
anti-UQCRC1, clone 16D10AD9AH5	Abcam	Cat# ab110252; RRID: AB_10863633
anti-UQCRC2, clone 14742-1-AP	Proteintech	Cat# 14742-1-AP; RRID: AB_2241442
anti-COX1, clone 1D6E1A8	Invitrogen	Cat# 459600; RRID: AB_10374492
Biological samples		
Human peripheral blood (healthy)	Clinica Universidad de Navarra	N/A
Chemicals, peptides, and recombinant proteins		
Liberase TL Research Grade	Sigma-Aldrich	Cat#5401020001
DNase I, Bovine Pancreas, > 2000U/MG	Biomatik	Cat#A4193
DAPI (4',6-Diamidino-2-Phenylindole, Dihydrochloride)	Thermo Fisher Scientific	Cat#D1306; RRID: AB_2629482

(*Continued on next page*)

Continued

REAGENT or RESOURCE	SOURCE	IDENTIFIER
Red Blood Cell Lysing Buffer Hybri-Max	Sigma-Aldrich	Cat#R7757
Oligomycin	Sigma-Aldrich	Cat#O4876
Carbonyl Cyanide 3-chlorophenylhydrazone (CCCP)	Sigma-Aldrich	Cat#C2759
Rotenone	Sigma-Aldrich	Cat#R8875
Antimycin A	Sigma-Aldrich	Cat#A8674
Myxothiazol	Sigma-Aldrich	Cat#T5580
Potassium cyanide	Sigma-Aldrich	Cat# 60178
Tetramethylrhodamine methyl ester perchlorate (TMRM)	Sigma-Aldrich	Cat#T5428
Dihydroethidium (DHE)	Sigma-Aldrich	Cat# D11347
LPS-EK	Invivogen	Cat# tlrl-eklps
R848	Invivogen	Cat#tlrl-r848-5
CpG ODN 1826	Invivogen	Cat# tlrl-1826-1
Poly(I:C) LMW	Invivogen	Cat# tlrl-picw
CellTrace Violet	Invitrogen	Cat# C34557
CellTrace CFSE Cell Proliferation Kit	Invitrogen	Cat# C34554
RPMI Medium 1640	Gibco	Cat#11875093
Sodium L-ascorbate	Sigma-Aldrich	Cat# A7631
Fibronectin bovine plasma	Sigma-Aldrich	Cat# F1141
Human Flt3-Ligand	Miltenyi Biotec	Cat# 120-096-474
Albumin from chicken egg white	Sigma-Aldrich	Cat# A5503
MHC class I $OVA_{257–264}$ (SIINFEKL)	GenScript	N/A
Saponin	Sigma-Aldrich	Cat# S4521
Paraformaldehyde (PFA) 16% (w/v)	Thermo Fisher	Cat# 28908
Dextran, Alexa Fluor647	Thermo Fisher	Cat# D22914
Dextran, pHrodo	Thermo Fisher	Cat# P35368
Critical commercial assays		
NAD/NADH-Glo Assay	Promega	Cat#G9071
Luminescent ATP Detection Assay Kit	Abcam	Cat#ab113849
RNeasy Micro Kit	QIAGEN	Cat# 74004
QIAamp DNA Mini Kit	QIAGEN	Cat# 51304
High-Capacity cDNA Reverse Transcription Kit	Applied Biosystems	Cat#4368814
GoTaq qPCR Master Mix	Promega	Cat#A6001
Seahorse XFe96 FluxPak	Agilent	Cat#103792-100
DNA Methylation Gold kit	Zymo Research	Cat# D5006
Deposited data		
Mouse bulk ATAC-seq data of splenic cDC1s or cDC2s from *Uqcrq*$^{f/f}$ or *Itgax-Uqcrq*$^{f/f}$ mice.	This paper	GEO: GSE276020
Mouse bulk RNA-seq data of splenic cDC1s or cDC2s from *Uqcrq*$^{f/f}$ or *Itgax-Uqcrq*$^{f/f}$ mice, stimulated or not in vivo with 50 μg poly(I:C) LMW and 50 μg R848 for 1.5 hours.	This paper	GEO: GSE276024
Mouse bulk DNA-methylation array of splenic cDC1s or cDC2s from *Uqcrq*$^{f/f}$ or *Itgax-Uqcrq*$^{f/f}$ mice.	This paper	GEO: GSE276025
Mouse bulk WGBS of splenic cDC1s from *Uqcrq*$^{f/f}$, *Itgax- Uqcrq*$^{f/f}$, *Uqcrq*$^{f/f}$ AOX-^{Rosa26} and *Itgax- Uqcrq*$^{f/f}$ AOX-^{Rosa26} mice.	This paper	GEO: GSE308685
Mouse bulk RNA-seq data of spleniccDC1s and cDC2s from the ImmGen project	http://www.ncbi.nlm.nih.gov/geo	GEO: GSE109125
Experimental models: Cell lines		
Mouse: B16-OVA melanoma	L. Chen, Yale University, New Haven, CT	N/A

(*Continued on next page*)

Continued

REAGENT or RESOURCE	SOURCE	IDENTIFIER
Mouse: B16-Flt3L	G. Dranoff, Harvard University, Boston, MA	N/A
Experimental models: Organisms/strains		
Mouse: CD45.1 (B6-SJL; Ptprc^{a} Pepc^{b}/BoyJ)	The Jackson Laboratory	RRID:IMSR_JAX:002014
Mouse: OT-II transgenic mice (C57BL/6-Tg (TcraTcrb)425Cbn)	The Jackson Laboratory	RRID:IMSR_JAX:004194
Mouse: *Uqcrq*$^{f/f}$ (Uqcrq$^{tm1.1Ncdl}$)	Weinberg et al.[23]	MGI: 6358198
Mouse: *Cox10*$^{fl/fl}$ (Cox10^{tm1Ctm})	Diaz et al.[25]	MGI:3605782
Mouse: *Aox*^{Rosa26}	Szibor et al.[44]	N/A
Mouse: *Tet2*$^{ko/ko}$ (B6(Cg)-*Tet2*$^{tm1.2Rao}$/J)	Fuster et al.[63]	MGI:175222
Mouse: *Itgax*^{Cre} (Tg(Itgax-cre)1-1Reiz)	Caton et al.[24]	MGI: 3763248
Oligonucleotides		
18S rRNA-sense (5′)–GTAACCCGTTGAACCCCATT–(3′); *18S rRNA*-antisense (5′)–CCATCCAATCGGTAGTAGCG–(3′)	Wculek et al.[28]	N/A
Uqcrq-sense (5′)–CTGTCCCAGGGCCGC–(3′); *Uqcrq*-antisense (5′)–AGATCAGGTAGACCACTACAAAC–(3′)	This paper	N/A
Cox10-sense (5′)–CACCACTGAAGAGGGTCAGC–(3′); *Cox10*-antisense (5′)–GATCCCTCCCAGAAGAAGCG–(3′)	This paper	N/A
Tet2-sense (5′)– AACCTGGCTACTGTCATTGCTC–(3′); *Tet2*-antisense (5′)– ATGTTCTGCTGGTCTCTGTGGGAA–(3′)	Fuster et al.[59]	N/A
Sdha (nDNA)-sense (5′)–TACTACAGCCCCAAGTCT–(3′); *Sdha (nDNA)*-antisense (5′)–TGGACCCATCTTCTATGC–(3′)	Matesanz et al.[64]	N/A
Mtco2 (mtDNA)-sense (5′)–CTACAAGACGCCACAT–(3′), *Mtco2 (mtDNA)*-antisense (5′)–GAGGGGGAGAGCAAT–(3′)	Matesanz et al.[64]	N/A
Recombinant DNA		
Secreted Flt3L-encoding plasmid (pUMVC3-mFLex)	Sanchez-Paulete et al.[65]	N/A
Software and algorithms		
ImageJ/Fiji	Schindelin et al.[66]	https://imagej.net/software/fiji/
GraphPad Prism version 9	GraphPad Software	https://www.graphpad.com
BD FACSDiva Software	BD Biosciences	https://www.bdbiosciences.com/
FlowJo v10	Tree Star	https://www.flowjo.com/
SDS software version 2.4 (Applied Biosystems 7900HT Fast Real-Time PCR System Software)	Thermo Fisher Scientific	https://www.thermofisher.com/
Seahorse Wave Desktop Software	Agilent technologies	https://www.agilent.com
R version 4.1.2	R CRAN	https://cran.r-project.org/
R package limma version 3.50.0	R Bioconductor	https://bioconductor.org/packages/release/bioc/html/limma.html
R package fgsea version 1.20.0	R Bioconductor	https://bioconductor.org/packages/release/bioc/html/fgsea.html
R package DiffBind version 3.12.0	Bioconductor	https://bioconductor.org/packages/DiffBind/
R package edgeR version 3.36.0	R Bioconductor	https://bioconductor.org/packages/release/bioc/html/edgeR.html
R package DSS version 2.50.1	Bioconductor	https://bioconductor.org/packages/DSS/
R package shinyEPICo	Bioconductor	https://bioconductor.org/packages/shinyepico/
R package sesame version 1.2	Bioconductor	https://bioconductor.org/packages/sesame/
Trim Galore version 0.6.10	Babraham Bioinformatics	https://www.bioinformatics.babraham.ac.uk/projects/trim_galore/
Samtools version 1.6	GitHub	https://github.com/samtools/samtools
Picard version 3.0.0	GitHub	https://github.com/broadinstitute/picard

(*Continued on next page*)

Continued		
REAGENT or RESOURCE	SOURCE	IDENTIFIER
Bowtie2 version 2.5.3	SourceForge	https://bowtie-bio.sourceforge.net/bowtie2/index.shtml
Genrich version 0.6.1	GitHub	https://github.com/jsh58/Genrich
RSEM version 1.3.3	N/A	https://github.com/deweylab/RSEM
HOMER version4.10	UCSD	http://homer.ucsd.edu/homer/
Ingenuity Pathway Analysis	QIAGEN	N/A
Other		
CD11c MicroBeads UltraPure, mouse	Miltenyi Biotec	Cat# 130-125-835
CD8+ Dendritic Cell Isolation Kit	Miltenyi Biotec	Cat# 130-091-169
Pan-DC Enrichment Kit, human	Miltenyi Biotec	Cat# 130-100-777
Streptavidin MicroBeads	Miltenyi Biotec	Cat# 130-048-102
LS Columns	Miltenyi Biotec	Cat# 130-042-401
MS Columns	Miltenyi Biotec	Cat# 130-042-201

EXPERIMENTAL MODEL AND STUDY PARTICIPANT DETAILS

Mice

Mouse colonies were bred at the CNIC under specific pathogen-free conditions and in C57BL/6 background. B6-SJL (Ptprc^{a} Pepc^{b}/BoyJ) mice expressing the CD45.1 allele were acquired from The Jackson Laboratory (Bar Harbor, ME, USA). OT-II transgenic mice (C57BL/6-Tg (TcraTcrb)425Cbn) were crossed with B6-SJL mice. *Uqcrq*$^{f/f}$ (Uqcrq$^{tm1.1Ncdl}$; MGI: 6358198),[23] *Cox10*$^{fl/fl}$ (Cox10^{tm1Ctm}, MGI:3605782),[25] *Aox*^{Rosa26} mice[44] that constitutively express the alternative oxidase (AOX) of *Ciona intestinalis*, and *Tet2*$^{ko/ko}$ mice (B6(Cg)-*Tet2*$^{tm1.2Rao}$/J; MGI:175222)[63] were previously reported. *Uqcrq*$^{f/f}$, *Cox10*$^{fl/fl}$ and *Aox*^{Rosa26} mice were crossed with *Itgax*^{Cre} (Tg(Itgax-cre)1-1Reiz; MGI: 3763248)[24] mice to generate *Itgax*Δ*Uqcrq*, *Itgax*Δ*Cox10* and *Itgax*Δ*Uqcrq Aox*^{Rosa26} mice. Mice were group-housed, have not been used in previous procedures and were fed standard chow diet. Littermates of the same sex were randomly assigned to experimental groups. 6–11 weeks old male and female mice were used for all experiments. All mice were maintained on a 12-hour light/dark schedule in a specific pathogen-free animal facility in individually ventilated cages and were given food and water ad libitum. Ambient temperature in the animal facility was 20–24 °C, and relative humidity was 45–65%. The local ethics committee approved all animal studies (PROEX172-19, 266.7_22). All animal procedures conformed to EU Directive 86/609/EEC and Recommendation 2007/526/EC regarding the protection of animals used for experimental and other scientific purposes, enforced in Spanish law under Real Decreto 1201/2005.

Human volunteers and blood sample collection

This study was approved by the Clinica Universidad de Navarra Ethics Committee (2019-039) and Navarra Blood and Tissue Bank Navarrabiomed Biobank. Written informed consent was obtained from all healthy and unrelated participants. We have complied with all relevant ethical regulations for obtaining blood samples from human participants, in accordance with the Declaration of Helsinki. A total of 5 Caucasian volunteers donated blood for this study.

METHOD DETAILS

Cell culture and mouse tumor models

B16-OVA (a kind gift from L. Chen, Yale University, New Haven, CT) were cultured at 37 °C in 5% CO_2 in R10 medium [RPMI Medium 1640 (Gibco®) with 10% heat-inactivated Fetal Bovine Serum (hi-FBS), 50 μM β-Mercaptoethanol (both Sigma), 2 mM L-Glutamine, 100 U/mL Penicillin and Streptomycin (100 μg both Lonza), 0.1 mM NEAA, 1 mM Sodium Pyruvate and 1 mM HEPES (all from HyClone)]. Cells were tested for absence of mycoplasma using the MycoAlert PLUS Mycoplasma Detection Kit (Lonza) according to manufacturer's instructions. Tumor cells were detached (5 mM EDTA/PBS) before reaching confluence and 4×10^5 B16-OVA cells were inoculated intravenously. Tumors growing in the lung were quantified by counting lung nodules under a stereomicroscope. Tumor cell lysate (TCL) was generated as previously described.[28] Briefly, B16-OVA cells were resuspended in R10 medium at 4×10^6 cells/ml, plated in a 6-well-plate and treated with ~300 mJ/cm^2 UV irradiation using a Stratalinker UV Crosslinker 1800 (Stratagene). Cells were cultured for 16-24 h at 37 °C in 5% CO_2, subjected to 3 freeze (− 80 °C) / thaw (37 °C) cycles of minimum 30 min each and passed through a 40 μm cell strainer before addition to cDC1s at a ratio of 1 cDC to 2 tumor cells.

In vitro mouse DC differentiation

FLDCs were generated as described.[67] Briefly, bone marrow cells were extracted by flushing the tibia and femur. Red blood cells were lysed by osmotic shock by 5 minutes exposure to red blood cell lysing buffer (Sigma). Cells were washed with R10, filtered through a 70 μm cell strainer and cultured at 37 °C in 5% CO_2 at approximately $1.5x10^6$ cells/ml in R10 supplemented with 50 ng/ml human Ftl3L (h-Flt3L) (Miltenyi Biotec). Media was refreshed on day 7 of the culture by adding 0.7 volume of R10 supplemented with 50 ng/ml h-Flt3L and floating cells were harvested on day 9. When indicated, sodium L-ascorbate (400 μM, Sigma) was added together with h-Flt3L.

Tissue dissociation

Spleen, inguinal lymph nodes (iLNs) and popliteal LN (popLN) were harvested in R10 medium. Spleen and LNs were digested for 10 min at 37 °C with 0.25 mg/ml Liberase TL (Roche) and 50 μg/ml DNaseI (Sigma). Tissues were squeezed through a 70 μm cell strainer (Corning), re-filtered through a 40 μm cell strainer and spleen subjected for 5 min to Red Blood Cell Lysis Buffer (Sigma).

Mouse dendritic cell *in vivo* expansion, enrichment and purification

When specified, cDC expansion was carried out via the inoculation of 2.5×10^6 B16-Flt3L cells in 100 μl PBS subcutaneously into both flanks of C57BL/6 mice and spleens harvested 10-11 days thereafter, as described previously.[28] Alternatively, and when indicated in the experiment, cDC expansion was conducted by hydrodynamic injection of 10 μg a secreted Flt3L-encoding plasmid (pUMVC3-mFLex) as described previously.[65]

For concomitant splenic cDC1s and cDC2s isolation, spleen single cell suspensions were subjected to positive selection of $CD11c^+$ cells using CD11c MicroBeads UltraPure (Miltenyi Biotec). Briefly, the single cell suspension was incubated for 15 minutes with CD11c MicroBeads in the presence of FcR block anti-mouse CD16/CD32 (2.4G2, Tonbo Biosciences), after which cells were purified using MACS columns and stained with antibodies (as specified below). Then, Fluorescence-Activated Cell Sorting (FACS) was to collect cDC1s ($MHCII^+CD11c^+CD8^+CD11b^-$) and cDC2s ($MHCII^+CD11c^+CD8^-CD11b^+$). When only cDC1s were used in the experiment, they were isolated using the mouse $CD8^+$ Dendritic Cell Isolation Kit using MACS columns and autoMACS Running Buffer according to manufacturer's instructions (Miltenyi Biotec) and as previously described.[28]

FLDC cDC1s or cDC2s were purified from FLDC cultures by incubation with FcR block anti-mouse CD16/CD32 and either biotinylated XCR1 (cDC1s) or biotinylated SIRPα (cDC2) antibodies in autoMACS Running Buffer (20 min at 4 °C) followed by incubation with Streptavidin MicroBeads (Miltenyi Biotec, 15 min at 4 °C) and magnetic purification using MACS columns.

Human peripheral blood dendritic cell enrichment

Peripheral blood mononuclear cells (PBMCs) were isolated by density gradient (Ficoll-Hypaque, Amersham Biosciences) from heparinized blood of healthy donors. Circulating DCs were enriched using the Pan-DC Enrichment Kit (Miltenyi Biotec) following the manufacturer's instructions and directly used in experiments.

In vivo and *ex vivo* activation of mouse and human DCs

For in vivo cDC stimulation, poly(I:C) LMW and R848 or the control PBS were intravenously (50 ug each) or intradermally (25 ug each) administered into *Uqcrq*$^{f/f}$, *Uqcrq*$^{f/f}$ *Aox*^{Rosa26}, *Itgax*Δ*Uqcrq* and *Itgax*Δ*Uqcrq Aox*^{Rosa26} mice and, after 1.5, 4, or 16 h, the spleen or iLN was harvested and processed for subsequent analyses (for example, for the analysis of surface molecules).

For ex vivo cDC stimulation, 2×10^5 pre-purified $CD11c^+$ cells from the mouse spleen were plated in round-bottom 96 well-plates and cultured in R10 with or without adjuvants (100 ng/ml LPS EK, 20 μg/ml poly(I:C) LMW, 5 μg/ml CpG ODN1826, 1 μg/ml R848) as specified in the experiment. After 4 h of culture, cells were stained with antibodies and analyzed by flow cytometry. When pharmacological inhibition of the ETC was used, $CD11c^+$ cells were incubated with ETC complex III inhibitors (antimycin A, 5nM or myxothiazol, 1nM) or complex IV inhibitor (KCN, 500 μM) starting 15 minutes before the addition of adjuvants.

For ex vivo stimulation of human circulating cDCs, $4x10^5$ pre-enriched cells were plated in round-bottom 96 well-plates and cultured in RPMI Medium 1640 (Gibco) with 10% heat-inactivated Fetal Bovine Serum (hi-FBS) and 100 U/mL Penicillin and Streptomycin (100 μg both Lonza). Cells were then treated or not with Antimycin A (5 nM) for 15 minutes followed by stimulation with adjuvants (20 μg/ml poly(I:C) LMW and 1 μg/ml R848). After 6 h of culture, cells were stained and analyzed by flow cytometry.

OT-II cell proliferation and *in vivo* assays

For ex vivo proliferation assays, splenic naïve $CD4^+$ OT-II T cells were purified from CD45.1 OT-II transgenic mice via FACS gating on $CD4^+$ $CD62L^+$ and $CD44^-$ cells. T cells were then labeled with CellTrace Violet Cell Proliferation Kit (Thermofisher, Molecular Probes) according to manufacturer's instructions. cDC1s or cDC2s from *Uqcrq*$^{f/f}$ or *Itgax*Δ*Uqcrq*$^{f/f}$ mice were FACS sorted from pre-purified $CD11c^+$ cells from the spleen and cultured for 1 hour in the presence of 20 ug/ml OVA protein (Sigma Aldrich), 20 μg/ml poly(I:C) LMW and 1 μg/ml R848 (all from InVivoGen) as specified in the experiment. cDCs were then washed with PBS and co-cultured with 10^4 labeled OT-II cells at a 1:1 ratio. After 5 days of co-culture, T cell proliferation was assessed by flow cytometry by dilution of the CellTrace Violet dye.

T cell re-stimulation assays measuring IFNγ expression

Single cell suspensions of spleen were re-stimulated ex vivo with MHC class I $OVA_{257–264}$ peptide (2 μM, GenScript) for 2 h in R10 at 37 °C in 5% CO_2 followed by 5 μg/mL Brefeldin A (Sigma Aldrich) treatment for 4 h. Cells were then labeled with the indicated surface-staining antibodies, fixed with 4% PFA (Thermofisher), permeabilized with 1% Bovine Serum Albumin, 0.1% Saponin, 0.02% Sodium Azide (all Sigma) in PBS and stained with anti-mouse IFNγ antibody (clone XMG1.2) from BioLegend.

Fluorescent staining, flow cytometry and cell sorting

Single cell suspensions of cells were incubated for 20 min at 4 °C in PBS with 2% FBS and 0.5 mM EDTA (Sigma) with FcR block anti-mouse CD16/CD32 (2.4G2, Tonbo Biosciences) and a mix of the following fluorochrome-conjugated antibodies (mouse): anti-mouse CD45.1 (clone A20), CD44 (clone IM7) and CD62L (clone MEL-14) from eBioscience, CD8 (clone 53–6.7), CD11b (clone M1/70), I-A/I-E (MHC-II, clone 2G9), SIRPα (clone P84), CD40 (clone 3/23), CD3 (clone 17A2) from BD Biosciences, CD11c (clone N418), XCR1 (clone ZET), B220 (clone C363-16A), CD80 (clone 16-10A1), CD45.2 (clone 104), CD90 (clone 53-2.1), CCR3 (clone J073E5), CCR7 (clone 4B12), OX40L (clone RM134L), PDL1 (clone 10F.962), CD19 (clone 6D5), CD24 (clone M1/69), B220 (clone RA3-6B2) and H-$2K^b$/H-$2D^b$ (MHC-I, clone 28-8-6) from BioLegend, CD86 (clone GL1) from Thermofisher, FOXP3 (clone FJK-16s) from Invitrogen and CD25 (clone PC61.5) from Tonbo Biosciences. Human cDCs were stained with antibodies (CD141, clone AD5-14H12) from Miltenyi Biotec, CD1c (clone L161), HLA-DR (clone L243) and CD80 (clone 2D10) from BioLegend and CD86 (clone 2331(FUN-1)) from BD Biosciences.

Staining with tetramethylrodamine (TMRM) or dihydroethidium (DHE, both Thermofisher) was performed as follows: cells were stained with antibodies and resuspended in RPMI Medium 1640 without phenol-red and supplemented with 50 μM β-Mercaptoethanol, 2 mM L-Glutamine, 100 U/mL Penicillin and Streptomycin, 0.1 mM NEAA, 1 mM Sodium Pyruvate and 1 mM HEPES containing 250 nM TMRM or 13 uM DHE, incubated for 30 (TMRM) or 45 (DHE) minutes at 37°C and analyzed without (TMRM) or following (DHE) washing.

Intracellular FOXP3 staining was performed using the Foxp3/Transcription factor staining kit from (Cytek Biosciences) following manufacturer's instructions.

DAPI (Sigma) was used to exclude dead cells. The LSRFortessa and FACSymphony cell analyzers and FACSAria and FACSFusion Cell Sorter (BD Biosciences) were used to record cells. FACSDiva software (BD Biosciences) and FlowJo version 10 were used to analyze data.

Nucleic acid (RNA or DNA) purification and qRT-PCR

Total RNA for all applications was extracted from cells with the RNeasy Micro Kit (Qiagen) and reverse transcribed using the HighCapacity cDNA Reverse Transcription Kit with random hexamers (Applied Biosystems) following manufacturer's instructions. Quantitative PCR was performed using the GoTaq qPCR Master Mix (Promega) in a 7900HT Fast Real-Time PCR System (Applied Byosystem). $2^{-\Delta Ct}$ mRNA expression values of mouse *Uqcrq* was calculated relative to expression of *18S rRNA*. *The following primers* (Sigma) *were used*: *18S rRNA*-sense (5′)–GTAACCCGTTGAACCCCATT–(3′); *18S rRNA*-antisense (5′)–CCATCCAATCGG-TAGTAGCG–(3′); *Uqcrq*-sense (5′)–CTGTCCCAGGGCCGC–(3′); *Uqcrq*-antisense (5′)–AGATCAGGTAGACCACTACAAAC–(3′); *Cox10*-sense (5′)–CACCACTGAAGAGGGTCAGC–(3′); *Cox10*-antisense (5′)–GATCCCTCCCAGAAGAAGCG–(3′); *Tet2*-sense (5′)–AACCTGGCTACTGTCATTGCTC–(3′); *Tet2*-antisense (5′)– ATGTTCTGCTGGTCTCTGTGGGAA–(3′).

Total DNA for all applications was purified from cells using the DNA mini kit (Qiagen) following manufacturer's instructions. The relative quantification of mitochondrial DNA (mtDNA) from FACS-sorted cDC1s or cDC2s from spleens of untreated $Uqcrq^{f/f}$ or *Itgax*Δ$Uqcrq^{f/f}$ mice was performed by qPCR assessing the relative abundance of the mitochondrially encoded gene *Mtco2* relative to the nuclear gene *Sdha*. The following primers (Sigma) were used: *Sdha (nDNA)*-sense (5′)–TACTACAGCCCCAAGTCT–(3′); *Sdha (nDNA)*-antisense (5′)–TGGACCCATCTTCTATGC–(3′); *Mtco2 (mtDNA)*-sense (5′)–CTACAAGACGCCACAT–(3′), *Mtco2 (mtDNA)*-antisense (5′)–GAGGGGGAGAGCAAT–(3′).

Extracellular flux analysis

The analysis of the extracellular acidification rate (ECAR) and oxygen consumption rate (OCR) were performed with an XF-96 Extracellular Flux Analyzer (Seahorse Bioscience). 2-3 x 10^5 cDC1s or cDC2s purified from FLDC cultures were plated in fibronectin-coated (5 μg/ml in PBS for 1 h, Sigma) Seahorse plates and cultured with adjuvants (20 μg/ml poly(I:C) LMW, 5 μg/ml CpG ODN1826 or 1 μg/ml R848) for 1, 4 or 20 h in reverse kinetics, as specified in the experiment. 3-4 x 10^5 $CD11c^+$ cells from the spleen of untreated mice were plated on Cell-Tak-coated (Corning) Seahorse plates and directly analyzed. Mito Stress test was performed on washed DCs in Seahorse medium [DMEM without glucose (Thermofisher) supplemented with 11.3 mM Glucose, 1 mM Sodium Pyruvate (HyClone), 2 mM L-Glutamine and 100 U/mL Penicillin and Streptomycin (both from Lonza) with pH adjusted to 7.4]. ECAR and OCR were monitored during the sequential injection of oligomycin (1 μM), FCCP (1 μM), and rotenone (1 μM) with antimycin A (1 μM). Basal respiratory rate (BRR), maximal respiratory rate (MRR) and spare respiratory capacity (SRC) were calculated as the average oxygen consumption before addition of oligomycin (BRR), average oxygen consumption after addition of FCCP (MRR) and the average difference between MRR and BRR (SRC).

Blue Native Gel Electrophoresis (BNGE)

For splenic cDC permeabilization, 5×10^6 $CD11c^+$ cells were resuspended in 100 μl of PBS. 32.5 μl of digitonin (4 mg/ml) was added and cells incubated on ice for 10 min. Cold PBS (1 ml) was added and cells were centrifuged for 5 min at 10,000x*g*. The pellet was suspended in 100 μl of AA buffer (500 mM 6-aminohexanoic acid, 50 mM imidazole, 1 mM EDTA, pH 7) and 10 μl of a 10% digitonin solution was added. Cells were centrifuged for 30 min at 18,000x*g*. Supernatant was harvested and 10 μl of sample buffer (5% Blue G-250, 5% glycerol in AA Buffer) was added. BN-PAGE was performed as described.[68] For densitometry analysis, the ImageJ2 software (v2.3.0) was used. Background correction was applied for each analysis. Anti-NDUFA9 (clone 20C11B11B11, Invitrogen) anti-SDHA (2E3GC12FB2AE2, Invitrogen), anti-UQCRC1 (16D10AD9AH5, Abcam), anti-UQCRC2 (14742-1-AP, Proteintech) and anti-COX1 (1D6E1A8, Invitrogen) antibodies were used to stain ETC complexes.

NAD+/NADH and ATP measurement

To measure NAD^+ and NADH we used the NAD/NADH-Glo assay (Promega) following the manufacturer's instructions. Briefly, 7.5×10^3 splenic cDC1s or cDC2s were washed with PBS and lysed in doddecyltrimethylammonium bromide (DTAB) and each sample divided in two. One of the replicas was treated with an acid solution (0.4N HCl) for 15 minutes at 60 °C to eliminate the reduced form NADH and the other replica was incubated in the basic DTAB solution for the specific elimination of the oxidized form NAD^+. Finally, NAD^+ or NADH relative abundance were detected upon incubation of the samples with a detection solution containing a NAD^+ cycling enzyme and a pro-luciferase that becomes functional upon reduction with NADH. Resulting bioluminescence was recorded.

Intracellular ATP content was determined in 2.5×10^4 splenic cDC1s or cDC2s from steady-state or poly(I:C) LMW and R848-stimulated mice (4-hour stimulation) using the Luminescent ATP Detection Assay Kit (Abcam) following the manufacturer's instructions.

DC migration assays *in vivo*

cDC1s and cDC2s were purified from spleens of B16-Flt3L tumor-harboring *Uqcrq*$^{f/f}$ or *Itgax*Δ*Uqcrq*$^{f/f}$ mice ($CD45.2^+$), cultured for 1 h in the presence of 20 μg/ml poly(I:C) LMW and 1 μg/ml R848 in R10, washed and 9×10^5 cells adoptively transferred into the footpad of CD45.1+ recipient mice (receiving either cDC1s or cDC2s). After 24 h, the popliteal lymph node was harvested, processed, and the presence of CD45.2 cDC1s and cDC2s quantified by flow cytometry.

Endocytosis and phagocytosis assay

2×10^5 pre-purified splenic $CD11c^+$ cells were plated in round-bottom 96 well-plates and cultured in R10 for 90 min in the presence or absence of 20 μg/ml poly(I:C) LMW and 1 μg/ml R848. To assess endocytosis, 50 μg/ml Alexa Fluor 647 dextran and 50 μg/ml pHrodo dextran (both Thermofisher) were added for 45 or 90 minutes at 4°C or 37°C, cells washed with HBSS containing 1 mM HEPES and fluorescence analyzed by flow cytometry. To assess phagocytosis, cells were cultured with labeled apoptotic B16-OVA cells for 60 minutes at 4°C or 37°C, washed and fluorescence analyzed by flow cytometry. To prepare the labeled apoptotic cells, B16-OVA cells were labeled with CFSE (Invitrogen) following the manufacturer's instructions and subsequently treated with ~300 mJ/cm^2 UV irradiation using a Stratalinker UV Crosslinker 1800 and cultured for 16 h at 37 °C.

Bulk RNAseq

Next generation sequencing experiments using total RNA from cDCs were performed in the Genomics Unit of the CNIC using the Illumina HiSeq 4000 System. Reads were mapped against reference transcriptome GRCm38.99 and quantified using RSEM using expected expression counts. Publicly available transcriptomic data of splenic cDC1 and cDC2 were obtained from GEO: GSE109125.[21] Data were then processed in R (v4.1.2) with a differential expression analysis pipeline that used the package *limma* for normalization and differential expression testing.

Genes were ranked according to log-fold change, gene set enrichment analysis was performed using FGSEA algorithm and KEGG databases and representation was done with barcode plots (depicting the running enrichment score of genes within the indicated pathway along the ranked genes by log-fold change) or histograms (displaying the normalized enrichment score (NES) of dysregulated pathways), all using R (v4.1.2). Over-representation analysis of pathways was performed using Ingenuity Pathway Analysis (IPA) (Qiagen).[69]

ATACseq

5×10^4 cDC1s or cDC2s were lysed by spinning at 500 x g for 20 minutes at 4°C in cold lysis buffer (10 mM Tris-HCl pH 7.4, 10 mM MgCl2, 0.1% IGEPAL CA-630). Nuclei pellets were resuspended in the transposase reaction mix (including 2 μl Transposase (Illumina)) and the transposition reaction was carried out for 1 h at 37 °C. Then, samples were purified using PCR Minelute kit (Qiagen) following the manufacturer's instruction and libraries generated by PCR using the NEBNext High-Fidelity PCR Master Mix (New England Biolabs) and the following PCR conditions: 72°C for 5 minutes, 98°C for 30 seconds, followed by thermocycling at 98°C for 10 seconds, 63°C for 30 seconds and 72°C for 1 minute for 12 cycles. The primers used for the library generation are reported elsewhere.[31] PCR product was purified using PCR Minelute kit (Qiagen) and SPRI beads-based size selection carried out using AMPure XP (Beckman). Libraries size and quality were assessed using a 2100 Bioanalyzer instrument (Agilent). Libraries were sequenced in paired-end reads (2×50) using a NextSeq 2000 System (Illumina) at the Genomics Unit of the CNIC.

Reads were trimmed to remove adapter contaminants and filtered out based on quality using TrimGalore. Then, reads were aligned to the reference genome GRCm38/MM10 using Bowtie2, and properly aligned reads were filtered out according to a mapping quality

greater than 30, not being aligned to mitochondrial DNA, and not being aligned to the ENCODE blacklist of problematic genomic regions.[70] Duplicated reads were removed and only those with a fragment size greater than 120pb (nucleosome-free regions) were kept for downstream analyses. Peak calling was performed using Genrich with ATAC-seq mode, and finally DiffBind was used to calculate and normalize the consensus peak set, and to identify differentially accessible regions (DARs) in pair-wise contrasts using EdgeR[71] as analysis method.

DNA methylation array and WGBS

For the DNA methylation array, DNA from cDC1s or cDC2s was bisulfite converted using the EZ DNA Methylation Gold kit (Zymo Research). Infinium Methylation BeadChip arrays (Illumina) were used to analyze DNA methylation, following the manufacturer's instructions. This platform allows around 850 000 methylation sites per sample to be interrogated at single-nucleotide resolution, covering 99% of the reference sequence genes. Quality control and analysis were performed using ShinyEPICo,[72] a graphical pipeline that uses minfi[64] for normalization, and limma[66] for differentially methylated positions (DMP) analysis. Cytosines were considered differentially methylated when the absolute differential of methylation was >5 % and the FDR was <0.1. TFME (Transcription Factor Motif Enrichment) analysis was conducted with HOMER software.[73] A flanking window of 250 bp was added to the DMP coordinates before calculating the enrichment.

For the WGBS, DNA from cDC1s was harvested using the DNA Micro Kit (Qiagen). Subsequent analysis was outsourced to the NGS Service of Macrogen Inc. Briefly, genomic DNA is bisulfite-treated, then sequentially adapter-tailed, extended, ligated, and amplified by indexing PCR to generate full-length libraries, with bead-based clean-ups at each step to remove small fragments and adjust buffer conditions. Reads were trimmed to remove adapter contaminants and filtered out based on quality using TrimGalore (v0.6.10) and aligned to the reference genome GRCm38/MM10 using BSMAP (v2.9). The only uniquely mapped reads are selected to sort, index and PCR duplicates are removed with SAMBAMBA (v0.5.9). The methylation ratio of every single cytosine location is extracted from the mapping results using BSMAP. The results of the coverage profiles were calculated as "# of C / effective CT counts" for each cytosine in CpG, CHH and CHG. Forward and reverse strands were collapsed to merge cytosine counts per genomic position, generating strand-independent CpG methylation estimates. Downstream analyses were performed following the default pipeline described in the DSS manual (v2.50.1) for the identification of differentially methylated loci (DML). DML comparisons were performed in a pairwise manner between experimental conditions, with smoothing enabled (smoothing = TRUE) to account for local correlation of methylation levels among neighboring CpG sites.

Liquid chromatography coupled to mass spectrometry (LC-MS) metabolic profiling

The LC-MS analysis was outsourced to VIB Metabolomics Core (Leuven, Belgium). Briefly, 1 mL of cold washing solution (0.9% NaCl) was added to $5x10^5$ purified splenic cDC1s or cDC2s (in vivo expanded with Flt3L-encoding plasmid), washed once, resuspended in 150 μl cold extraction buffer (MeOH:H2O, 8:2, v:v), subjected to brief vortex-mixing and frozen. 10 μl of each sample was loaded into a Dionex UltiMate 3000 LC System (Thermo Scientific Bremen, Germany) equipped with a C-18 column (Acquity UPLC -HSS T3 1.8 μm; 2.1 x 150 mm, Waters) coupled to a Q Exactive Orbitrap mass spectrometer (Thermo Scientific) operating in negative ion mode. A step gradient was carried out using solvent A (10 mM TBA and 15 mM acetic acid) and solvent B (100% methanol). The gradient started with 0% of solvent B and 100% solvent A and remained at 0% B until 2 min post injection. A linear gradient to 32.3% B was carried out until 7 min and increased to 36.3% until 14 min. Between 14 and 26 minutes the gradient increased to 90.9% of B and remained at 90.9% B for 4 minutes. At 30 min the gradient returned to 0% B. The chromatography was stopped at 40 min. The flow was kept constant at 0.25 mL/min and the column was placed at 40°C throughout the analysis. The MS operated in full scan mode (m/z range: [70.0000-1050.0000]) using a spray voltage of 4.80 kV,capillary temperature of 300 °C,sheath gas at 40.0, auxiliary gas at 10.0. The AGC target was set at 3.0E+006 using a resolution of 70000, with a maximum IT fill time of 512 ms. Data collection was performed using the Xcalibur software (Thermo Scientific). The data analyses were performed by integrating the peak areas (El-Maven – Polly - Elucidata). Differential abundance analysis was performed using the *limma* package (R). Blank values were subtracted for each metabolite, and only metabolites with values above the limit of detection in all samples (defined as blank value + 3 × SD) were retained. A linear model was fitted to the abundance data for each metabolite, and predefined contrasts of interest were specified. Moderated t-statistics, log-odds of differential expression, and associated p-values were computed using empirical Bayes moderation of the standard errors. P-values were adjusted for multiple testing using the Benjamini–Hochberg method.

QUANTIFICATION AND STATISTICAL ANALYSIS

Data analysis employed GraphPad Prism version 10.0 and R for omic analyses (see details above). Data are presented as mean ± standard error of the mean and were analyzed, as indicated in the figure legends, using Two-tailed Student's t-test (Paired or unpaired according to experimental setting), one-way ANOVA (or mixed effect model when matched data is analyzed) and Tukey post hoc test and Two-way ANOVA. All experiments were repeated at least twice and either representative experiments or pooled data from several experiments are shown as indicated in the Figure legends. Mice were allocated randomly in different experimental groups. All *n* values represent biological replicates (different mice, primary cell preparations or in vitro experiments).